ACS Sustainable Chemistry & Engineering

pubs.acs.org/journal/ascecg

Research Article

# PLA–Potato Thermoplastic Starch Filament as a Sustainable Alternative to the Conventional PLA Filament: Processing, Characterization, and FFF 3D Printing

Agnieszka Haryńska,* Helena Janik, Maciej Sienkiewicz, Barbara Mikolaszek, and Justyna Kucińska-Lipka

Cite This: https://doi.org/10.1021/acssuschemeng.0c09413

Read Online

ACCESS | Metrics & More | Article Recommendations | Supporting Information

**ABSTRACT:** The growing popularity of the fused filament fabrication (FFF) 3D printing technology in science, industry, and in-home use is associated with an increased demand for high-quality polymer filaments. This study presents an in-depth characterization and analysis of a self-made bio-based polylactide (PLA)/thermoplastic potato starch (TPS) filament dedicated for the FFF 3D printing technology. The obtained results were compared with the commercial PLA filament (FF). The series of conducted studies (i.e., Fourier-transform infrared spectroscopy, Raman spectroscopy, differential scanning calorimetry, thermogravimetric analysis, and dynamic mechanical analysis) revealed that both of the investigated filaments are stable under FFF 3D printing conditions. The mechanical test showed a correlation between the print orientation and raster angle on the strength features. The most favorable strengths values were recorded for the *ZX*_0° configuration, which were ∼18/22 MPa of tensile strength and ∼9/18 kJ $m^{-2}$ of Charpy impact strength for the PLA/TPS filament and FF, respectively. Also, it was observed that the developed bio-filament has a more hydrophilic surface and is more susceptible to hydrolytic degradation in the phosphate-buffered saline solution than the FF. The composting study (according to the EN ISO 20200 standard) revealed that the commercial PLA printouts remain intact, while the PLA/TPS samples showed a mass loss of 19%. Finally, the remarkable printability of PLA/TPS was successfully demonstrated by FFF 3D printing of personalized anatomical models and complex porous structures.

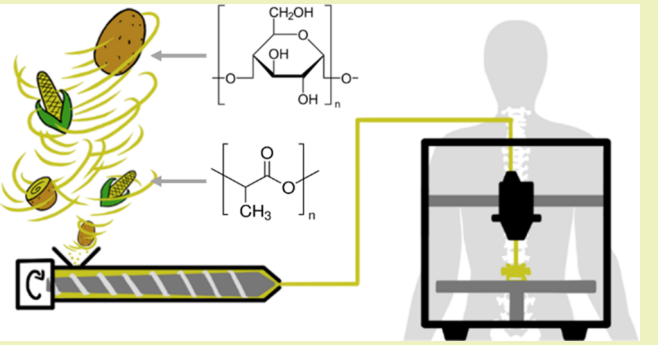


**KEYWORDS:** *fused filament fabrication, 3D printing, potato thermoplastic starch, polylactide, material characterization, bio-based filaments*



## INTRODUCTION

The use of additive manufacturing (AM) technologies in industry and science has become widespread nowadays. These methods are irreplaceable in rapid prototyping as well as more and more often used in the production of finished products. The example of the AM technologies that is particularly popular in the industry, medicine, and home use is the fused filament fabrication (FFF). This highly available technology primarily uses thermoplastic-based polymers as the raw material. The most popular materials (filaments) for FFF 3D printing (3DP) are acrylonitrile butadiene styrene (ABS), polylactide (PLA), polyamide (PA), and thermoplastic elastomer (TPE).[1] Nevertheless, along with the growing interest in this molding method, the amount of petrochemical polymers used is constantly increasing. As prototyping involves the formation of disposable products, the amount of FFF 3D-printed waste reaches a very alarming level. While the recycling of unmodified thermoplastics is not regarded as a problem, the effective recovery of raw materials from modified 3D printout waste (blends and composites) is much more difficult. Therefore, new solutions on fossil fuels-based filament substitutes with less negative environmental impact are being sought.[2]

More and more attention is being paid to the development of bio-filaments for FFF 3DP, which are based on materials that are biodegradable and/or obtained from renewable resources. The most recent literature reports regarding this topic are presented in Table 1. The developed materials are, in most cases, PLA-based composites modified with natural powders (walnut shell powder[4]) or managed eco-wastes (spend coffee grounds[5] and spruce pulp fibers[3]). Other studies focus on the use of recyclates as efficient feedstocks for FFF 3D printers. Idrees et al.[6] proposed a filament based on waste polyethylene terephthalate

Received: January 2, 2021
Revised: March 29, 2021

**Table 1. Latest Literature Reports on Bio-Filaments for 3D Printing in the FFF Technology**

| bio-filaments | | | | | |
|---|---|---|---|---|---|
| type of filament | composition | short description | material properties[b] | suggested application | refs |
| fiber-based composites | PLA/TMP[a] | development of biocomposite filaments of PLA with modified spruce thermomechanical pulp fibres (TMP) (10 and 20 wt %) | tensile strength = 10−23 MPa, water contact angle of selected samples up to 100° (highly hydrophobic properties) | antibacterial 3D-printed devices | 3 |
| particle-based composites | PLA/WSP[a] | studies of bio-based composite filaments based on the PLA matrix with a walnut shell powder (WSP) modifier (5 wt %) | melt flow index (MFI, 160 °C, 3.8 kg) = 8−18 g 10 $min^{-1}$, compressive strength = 212−276 MPa, Young modulus = 2.5−3.0 GPa, tensile strength = 48−52 MPa | trabecular bone tissue scaffolds | 4 |
| | PLA/Ox-SSG[a] | fabrication and characterization of bio-based PLA filaments loaded with oil-extracted spent coffee grounds (Ox-SCG) (5−20 wt %) | toughness = 5−25 MJ $m^{-3}$ | personalized prosthesis | 5 |
| | PET/Biochar | development of sustainable filaments from recycled PET bottles enhanced with biochar derived from packaging waste (0.5−5 wt %) | Young modulus = 0.7−09. GPa, tensile strength = ∼50 MPa | a sustainable, recycle-based alternative for automotive and engineering application | 6 |
| nanocomposite | PA-11/sepiolite nanoclay[a] | development of fully biorenewable filaments based on a PA-11 monomer (11-amino-undecanoic, castor beans origin) modified with natural clay (1, 3, and 7 wt %) | Young modulus = 0.7−1.15 GPa, tensile strength = 27−47 MPa, strain at break = 5−38% | biorenewable alternative to PLA filaments with higher printing temperature for engineering application | 7 |
| | PHBH/CNC[a] | studies of bio-based PHBH filaments modified with functionalized cellulose nanocrystals (CNC) (5−20 wt %) | disintegration ratio in a laboratory-scale composting test (60th day of the test) = 55−80% | external medical devices, surgical implants, tissue scaffolds | 8 |
| polymer blends | TPS/ABS | development of partly bio-based filaments composed of 30 wt % debranched-with-α-isoamylase thermoplastic starch (TPS) and acrylonitrile butadiene styrene (ABS) | impact strength (Izod, notched) = 8−18 J $m^{-1}$, flexuralmodulus = 2.1−2.5 GPa, tensiles-trength = 34−48 MPa | household gadgets, inductrial design, architecture | 9 |
| | PBS/PLA | fabrication and characterization of biodegrad-able filaments consisting of the mixture of PBS with PLA (20−60 wt %) | tensile strength = 16−21 MPa | architectural design | 10 |
| | PLA/PBAT | formulation of biofilaments with increased impact strength from PLA-based blends containing 10, 20, and 30% of poly(butylene adipate-*co*-terephthalate (PBAT) | Impact strength (Izod, notched) = 30−719 J $m^{-1}$, Young modulus = 2.2−3.0 GPa, tensile strength = 40−63 MPa, elongation at break = 7.6−84% | not specified | 11 |

[a]Fully bio-based. [b]The given mechanical properties refer to FFF 3D printouts made using developed filaments.

(PET) bottles with the addition of biochar (derived from packaging waste) as a sustainable alternative to conventional filaments. Another interesting solution seems to be a modification of poly(3-hydroxybutyrate-*co*-3-hydroxyhexa-noate) (PHBH) with cellulose nanocrystals (CNC), proposed by Giubilini et al.[8] As a result, a printable FFF filament with enhanced thermal and mechanical properties as well as improved compostability was obtained. This product combines both compostability and fully renewable origin; therefore, it can be considered as "double green". However, the relatively high production costs of PHBH and CNC may hamper the introduction of this product at an industrial scale. Thus, nowadays, it seems reasonable to follow the "double-ECO" approach proposed by Tanabe[12] which takes into consideration not only the environmental and ecological issues but also an economical aspect of the production.

In our previous research, we developed a biodegradable and compostable polymer composition based on renewable and natural-origin ingredients.[13] The composition consists of PLA and thermoplastic potato starch (TPS) modified with epoxidized soybean oil (ESO). As a result, we improved PLA's ductility as well as reduced the costs of the granulate without compromising biodegradability and compostability. In the next step, we started research on the use of the developed composition as a sustainable material for FFF 3DP. Therefore, in this study, we present the full characteristics of self-made PLA/TPS filament which can be a sustainable alternative to the commonly used petrochemical filaments. Moreover, to facilitate direct comparison of the formed PLA/TPS filament with commercially available products, all of the presented studies were also carried out for the FlashForge PLA filament. The schematic flowchart showing the steps of the work is presented in Figure 1. Structural, thermal, and mechanical properties, as well as wettability, susceptibility to hydrolysis, and disintegration in composting conditions, were evaluated. Furthermore, spectroscopic and thermal studies were carried out for both

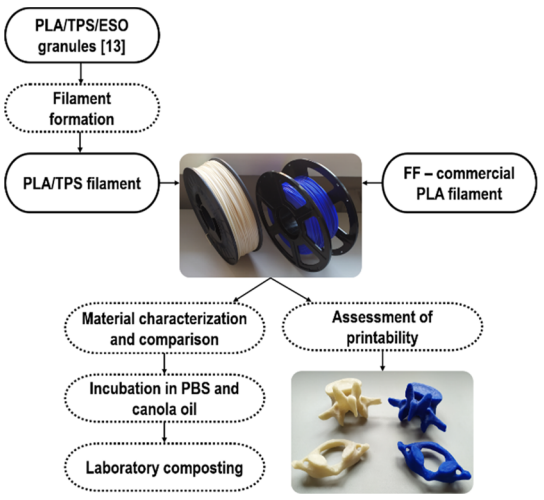


**Figure 1.** Schematic flowchart representing the steps of the work.





https://doi.org/10.1021/acssuschemeng.0c09413
ACS Sustainable Chem. Eng. XXXX, XXX, XXX−XXX

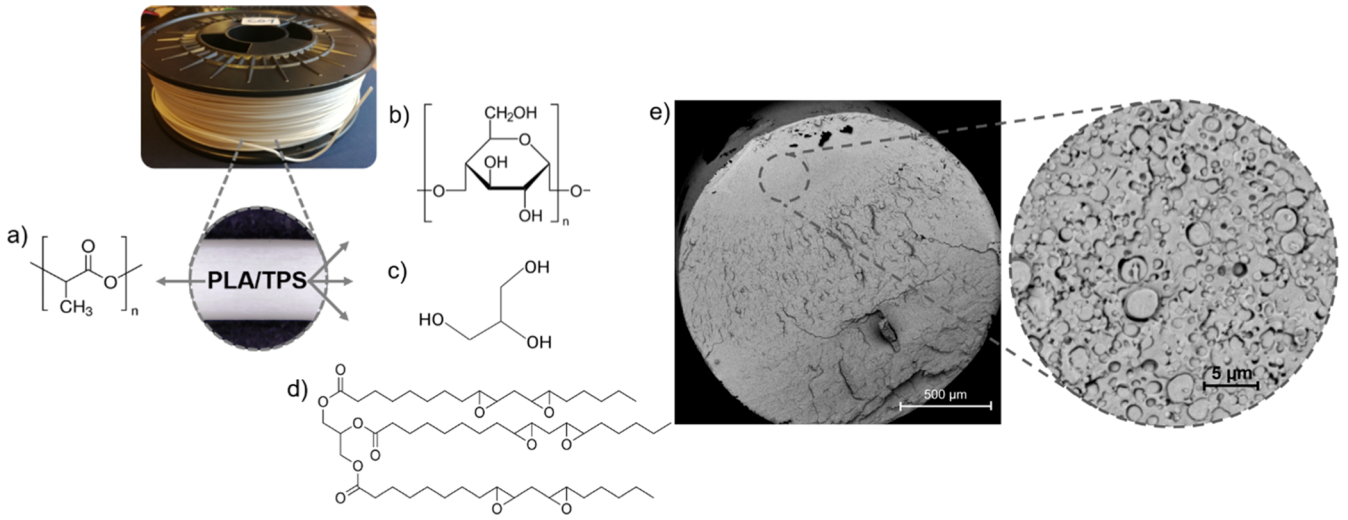


**Figure 2.** Scheme of the PLA/TPS filament composition: (a) PLA, (b) potato starch, (c) glycerin, and (d) ESO and (e) SEM image of the PLA/TPS filament (in cross-section view).

filaments and the formed printouts to assess the stability of the material under FFF 3DP conditions. Finally, the FFF printability of the proposed novel bio-filament was evaluated and compared with that of commercial PLA printouts. For this purpose, we printed (FFF 3DP) personalized anatomical models (cervical and lumbar vertebrae) and complex-shaped porous structures (gyroid and cancellous bone-like structure). To our best knowledge, we have not found so far any literature reports on PLA-based filaments modified with TPS for FFF 3DP. Thus, the presented research may be an interesting offer for other scientists or industries looking for bio-based filaments with increased compostability and adequate printability.

## EXPERIMENTAL SECTION

**Materials.** The PLA/TPS granulate used to obtain the PLA/TPS_F filament was previously developed and described in detail in our earlier article.[13] The composition selected for this work contained fully plant-based-origin biodegradable raw materials, that is, 60 wt % PLA (7032D transparent injection grade, NatureWorks, USA, MFR = 7 g 10 $min^{-1}$ at 210 °C and 2.16 kg) and 40 wt % TPS (Figure 2). TPS was obtained by melt extrusion of the following mixture: native potato starch (ZetPezet, Poland, humidity 16%), plant pharmaceutical-grade glycerin, used as a plasticizer (TechlandLab, Poland, $\rho$ = 1.26 g $cm^3$), and ESO (Brenntag, Germany), which served as a reactive modifier. The wt % ratio of the TPS components was as follows: potato starch 65.7%; glycerin 33.3%; and ESO 1%.

A wildly available commercial PLA filament produced by FlashForge (Zhejiang, China) was selected as the reference material. The FlashForge PLA filament (FF) (blue colour, Ø = 1.75 mm) is characterized by the producer in terms of printing conditions (printing temperature: 190−220 °C and bed temperature: 50−60 °C) and basic material properties (density: 1.24 g $cm^{-1}$, yield strength: 62 MPa, tensile break: 15%, and impact strength: 4.2 kJ $m^{-2}$). It is also described as environmentally friendly and biodegradable. According to the material safety data sheet, the FF contains 95% of PLA, 4% of TPE, and 1% of additives in the form of mineral oils. Symbols and description of studied materials are presented in Table 2.

**Filament (PLA/TPS_F) Formation.** The filament-forming system used to obtain the PLA/TPS filament (Ø = 1.75 mm) consisted of a granulator dryer (50 °C/5 h), a single-screw extruder ($L/D$ = 32, with three heating barrel zones and two head zones), two cooling tubes filled with water (40 °C/22 °C) and equipped with calibrators (Ø = 2 and 1.8 mm), a laser diameter measurement system (laser sensor accuracy 0.01 mm), the puller (pulling velocity ∼70 rpm), and a spool winding system. The extrusion temperature profile of barrels zones was I—140 °C, II—160 °C, and III—168 °C and for head zones IV—170 °C and V—172 °C. The temperature of the melt was 176 °C, the head pressure was 21 ± 2 bar, and the extrusion velocity was set at 35 rpm. The scheme and detailed description of the applied filament-forming system are presented in our previous article.[14]

**Table 2. Symbols and Description of Materials Used in the Study**

| | | composition (wt %) | | | |
|---|---|---|---|---|---|
| | | | TPS | | |
| symbol | description | PLA | potato starch | plant glycerin | ESO |
| PLA/TPS_F | filament | 60 | 26.3 | 13.3 | 0.4 |
| PLA/TPS_P | printout | | | | |
| symbol | description | PLA | thermoplastic elastomer | | mineral oils |
| FF_F | filament | 95 | 4 | | 1 |
| FF_P | printout | | | | |

**3D Printer, Test Samples, Anatomical Model Design, and 3D Printing Settings.** Prusa i3 MK3S (Prusa Research, Prague, Czech), an FFF-based 3D printer, with PrusaSlicer software (2.20 version) was used to print the studied details. Autodesk Inventor software (Autodesk, Warszawa, Poland) was used to prepare SLT files of test specimens (for tensile, compression, and impact tests). The 3D printing settings of all test samples used for characterization are listed in Table S1, and dimensions of samples for strength tests are presented in Figure S1 (the Supporting Information). The L3 and C1 vertebrae were selected as exemplary anatomical models, while the gyroid and cancellous bone were selected as porous structures. Vertebrae models L3 and C1 were prepared by the segmentation of the CT scan of the spine of a healthy woman. The segmentation process was conducted via 3D Slicer software (https://www.slicer.org/, 4.10.2 version). 3D Slicer is an open-source software platform for visualization and medical image computing.[15] The scheme of the segmentation procedure of personalized anatomical models is presented in Figure S2. In turn, the description of porous models (the gyroid and cancellous bone) and detailed 3D printing settings are shown in Tables S2 and S3 (the Supporting Information).

**Characterization of the Filaments and Printouts.** A series of studies including spectroscopy [Fourier-transform infrared (FTIR) and Raman], X-ray diffraction (XRD), thermal studies [differential scanning calorimetry (DSC) and thermogravimetric analysis (TGA)], dynamical mechanical analysis (DMA), melt flow rate (MFR) measurements, mechanical properties tests (tensile, Charpy impact, and compression tests), and water contact angle (wCA) measurements




https://doi.org/10.1021/acssuschemeng.0c09413
ACS Sustainable Chem. Eng. XXXX, XXX, XXX−XXX

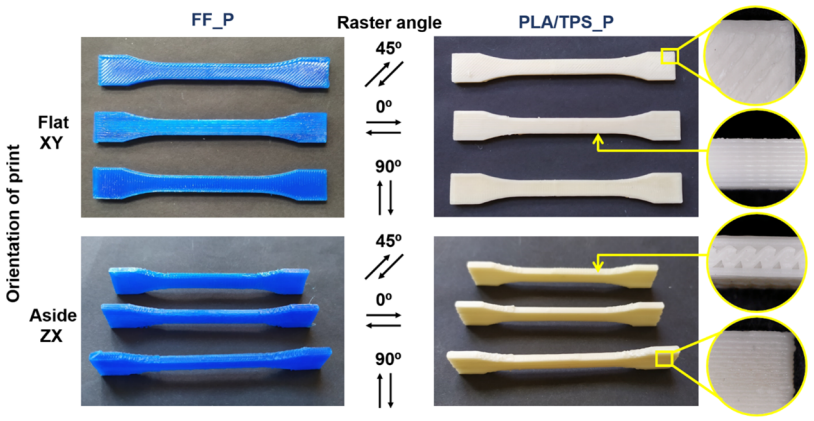


**Figure 3.** View of the build orientation and raster angle of test specimens.

were conducted on both materials to characterize and compare the FF with the self-made PLA/TPS one.

**Spectroscopic Studies.** The infrared spectra of the samples were collected via an attenuated total reflectance FTIR Nicolet 8700 spectrometer (Thermo Fisher Scientific, Waltham, USA). The spectral range was 4000−500 $cm^{-1}$, resolution 4 $cm^{-1}$, and 64 scans per measurement. The study was carried out at room temperature. The Raman spectra were obtained using a confocal micro-Raman system (inVia, Renishaw, UK) equipped with a red laser (785 nm) operating at 50% of the total power (50 mW).

**XRD Analysis.** XRD analysis was conducted via the Rigaku Intelligent X-ray diffraction system SmartLab (Rigaku Corporation, Tokyo, Japan) equipped with a sealed tube X-ray generator (a copper target; operated at 40 kV and 30 mA). Data were collected in the $2\theta$ range of 5−50° with a scan speed of 2° $min^{-1}$ and a scan step of 0.01°.

**Thermal Properties.** Thermal characteristic was studied by DSC and TGA. DSC measurements were collected using a Netzsch 204F1 Phoenix apparatus (Netzsch, Germany) under a nitrogen atmosphere (20 ml $min^{-1}$) at the temperature range of 25−220 °C and a heating/cooling rate of 5 °C $min^{-1}$. The sample weight was ∼6 mg. In turn, a Netzsch TG 209 instrument (Netzsch, Germany) was used to collect TGA data. The temperature range was 35−600 °C with a heating rate of 10 °C $min^{-1}$ under a nitrogen atmosphere (sample weight ∼7 mg). The degree of PLA crystallinity ($X_{c\ PLA}$) was calculated based on the following formula 1

$$X_{c\ PLA}\ (\%) = \left(\frac{\Delta H_m - \Delta H_{cc}}{\Delta H_m^0}\right) \times \frac{1}{w_{PLA}} \times 100\% \quad (1)$$

where $\Delta H_{cc}$, $\Delta H_m$, and $\Delta H_m^0$ represent the heat of cold crystallization, heat of melting, and melting of 100% crystalline PLA (93 J $g^{-1}$[16]), respectively. The $1/w_{PLA}$ factor takes into account the actual content of PLA in the tested samples.

**Dynamic Mechanical Analysis.** The dynamical mechanical test was performed via a DMA Q800 analyzer (TA Instruments, USA) under the single cantilever bending mode with 1.0 Hz frequency of an oscillatory deformation (sample dimension 40 × 10 × 2 $mm^3$). The temperature range was −100 to 130 °C (heating rate 4 °C $min^{-1}$).

**Rheological Properties.** The MFR and melt volume rate (MVR) of the samples were measured by a Zwick/Roell load plastometer (M-Flow, BFN-001, Zwick, Poland) in accordance with the ISO 1133:2005 standard. The measurement was conducted at four different temperatures (180, 190, 200, and 210 °C) under a load of 2.16 kg. Five repetitions were made for each sample, and the result was presented as an average ($n$ = 5).

**Water Contact Angle.** The wCAs of the samples were determined with a ramé-hart 90-U3 goniometer and DROPimage Pro software (ramé-hart, USA). Before measurements, the sample surface was degreased and a 2 $\mu$L droplet of deionized (DI) water was deposited. Then, the images were collected. Six repetitions were made for each sample, and the result was calculated as an average ($n$ = 6). The test was carried out on flat surfaces of the printouts (infill density = 100% and raster angles of 0 and 90°).

**Mechanical Properties.** The hardness of the printed samples was measured using the Shore D-type durometer (Zwick/Roell, Germany) according to the ISO 868 standard. Fifteen repetitions per sample were made, and the results were averaged. The tensile tests were performed on printed dumbbell-shaped specimens using a Zwick/Roell Z020 universal tensile machine equipped with an adapter for determining the Young modulus. The measurements were carried out according to the ISO 527 standard at room temperature. The cross-head speed was 5 mm $min^{-1}$, and the initial force was 1 N. At least six samples were tested, and results were averaged. The Charpy impact strength was determined using a pendulum impact tester (Zwick/Roell HIT5.5P) with a 5 J hammer according to the ISO 179 standard (unnotched). The uniaxial compression test was carried out on cubic specimens via a Zwick/Roell Z020 machine. Samples were compressed until 25% strain was reached at a rate of 5 mm $min^{-1}$ (five samples per series). The brittleness (B) of samples was calculated based on eq 2 formulated by Brostow et al.[17]

$$B = \frac{1}{\varepsilon_b \times E'} \quad (2)$$

where $\varepsilon_b$ (%) is the tensile elongation at break and $E'$ (Pa) represents the value of the storage modulus (at a temperature of 25 °C) which was determined by DMA. To facilitate the presentation of the obtained values, the brittleness is expressed as (% Pa $10^{-10}$).

Detailed information on test specimen design and dimensions are shown in Figure S1. The tensile and impact tests, as well as brittleness, were rated depending on the infill raster angle (0, 45, and 90°) and the orientation of the printout in relation to the plane of the printer's build table (flat $XY$ and aside $ZX$) (Figure 3).

**Degradation Studies.** Filaments (FF_F and PLA/TPS_F) were incubated in 0.1 M phosphate-buffered saline (PBS, Sigma-Aldrich) and food-grade canola oil for 30 days at 37 °C. The filaments were cut into pieces (∼3 mm length) and then dried and weighed ($m_0$) in a thermobalance (Radwag MAX50/SX, Radom, Poland) at 60 °C. Thus, the prepared samples were placed in 50 mL polypropylene Falcon tubes and immersed with 35 mL of the appropriate medium. Three samples per series were tested, and results were averaged. At each respective time point (1 h, 5 h, 1, 3, 7, 14, and 30 days), samples were carefully removed. In the case of PBS incubation, samples were further rinsed with DI water and dried in a laboratory oven at 50 °C for 48 h. Subsequently, the pH of PBS residues was also monitored (pH-100 ATC, Voltcraft, Germany). Mass loss (Ms) was calculated as follows 3

$$M_s\ (\%) = \frac{m_0 - m_x}{m_0} \times 100\% \quad (3)$$

where ($m_0$) is the initial mass of the sample and ($m_x$) is the residual mass.

Furthermore, incubation in 0.1 M PBS was monitored by FTIR measurements and a scanning electron microscope (Phenom Pro Generation 5, Thermo Fisher, Eindhoven, Netherlands, AV = 5 kV).





https://doi.org/10.1021/acssuschemeng.0c09413
ACS Sustainable Chem. Eng. XXXX, XXX, XXX−XXX

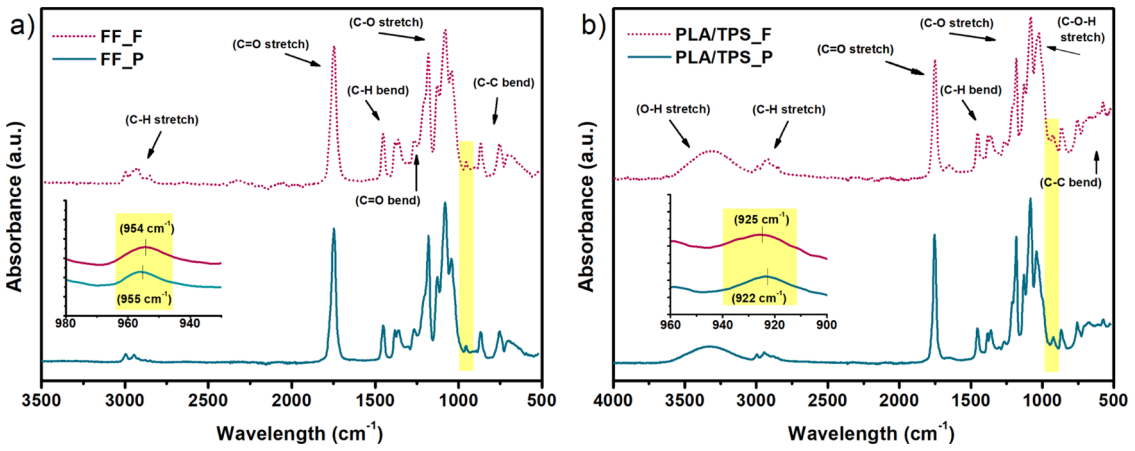


**Figure 4.** FTIR spectra of (a) FF and (b) PLA/TPS filaments and printouts.

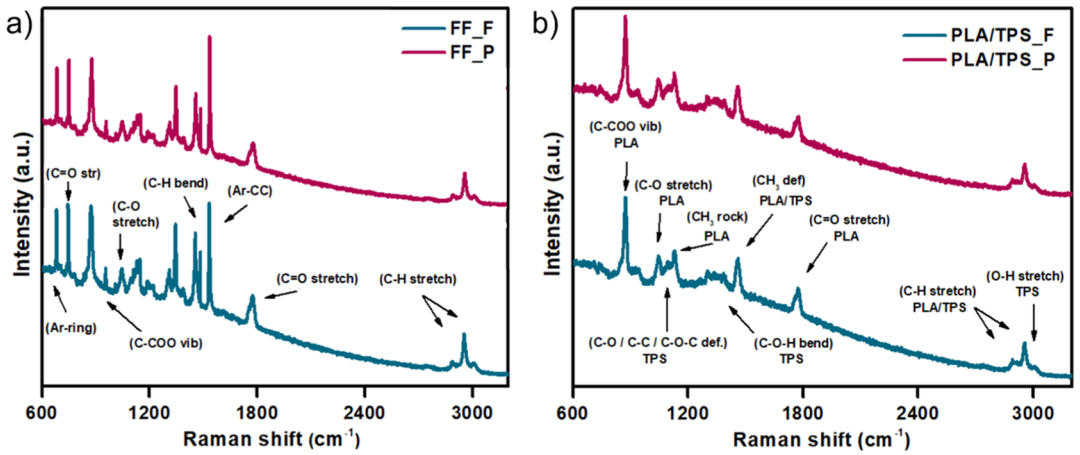


**Figure 5.** Raman spectra of (a) FF and (b) PLA/TPS filaments and printouts.

In the case of incubation in canola oil, in addition to the mass loss, the degree of swelling (Sw %) was also determined. For this purpose, after removing the sample from the medium, excess oil was gently removed from the surface with a paper towel, and then, the sample was weighed. The Sw % was calculated based on the following formula 4

$$\text{Sw}\ (\%) = \frac{m_x - m_0}{m_x} \times 100\% \tag{4}$$

**Laboratory-Simulated Composting.** Evaluation of the degree of disintegration of the printouts (FF_P and PLA/TPS_P) under a laboratory-scale composting environment was carried out according to the EN ISO 20200 standard. The composition of the composting mixture is given in Table S4. The initial pH of the compost was 5.95 and relative humidity over 90% (water was added periodically to the containers during the test according to the procedure given in the ISO standard to ensure constant humidity). Printed samples with the dimensions of 1.5 cm length, 1 cm width, and 2 mm thickness were tested (three samples for each material). The samples were dried (60 °C, 48 h) and weighed before testing. Then, the samples were put in polypropylene reactors filled with compost and placed in a bioreactor (48 °C for up to 60 days). To ensure aerobic conditions, the containers were opened and flipped each week. At each time interval (7, 14, 30, 50, and 60 days), samples were carefully removed, rinsed with DI water, dried, and weighed. The degree of disintegration ($D$ %) was calculated based on mass loss measurements (eq 5), where ($m_0$) is the initial mass of the sample and ($m_y$) is the dry mass of the tested sample at different composting periods. The composting process was monitored via mass measurements, optical photos of the sample's surface (magnification ×20, Delta Optical Generic, Pro, Mińsk Mazowiecki, Poland), scanning electron microscopy (SEM), and FTIR spectroscopy.

$$D\ (\%) = \frac{m_0 - m_y}{m_0} \times 100\% \tag{5}$$

## RESULTS AND DISCUSSION

**Structural Characterization (FTIR Spectroscopy, Raman Spectroscopy, and XRD).** The results of the FTIR studies are shown in Figure 4. Spectroscopic studies were conducted on both filaments (FF_F and PLA/TPS_F) and printouts (FF_P and PLA/TPS_P) to evaluate the structural stability during the FFF 3D printing (3DP) process.

Analyzing the spectrum of the commercial filament (FF_F), the presence of functional group characteristics for PLA was noted (Figure 4a). The absorption band visible in the range of 2380−3010 $cm^{-1}$ corresponds to the symmetric and asymmetric stretching of the $CH_3$ group. The C═O stretching vibration occurred at 1748 $cm^{-1}$. The band at 1452 $cm^{-1}$ is attributed to the $CH_3$ asymmetric bending vibration. The band at 1264 $cm^{-1}$ is associated with the C═O bending vibration, whereas the bands at 1179, 1083, and 1043 $cm^{-1}$ correspond to the C−O−C stretching vibration of PLA-ester groups. In turn, the spectrum of the PLA/TPS filament shows additional bands derived from TPS, that is, a broad signal at 3310 $cm^{-1}$ (O−H stretching vibration), a band at 1020 $cm^{-1}$ (deformation of C−O, glucose ring), and signals in the region of 1080−1100 $cm^{-1}$ (C−O stretching of the C−O−H group).[18]





https://doi.org/10.1021/acssuschemeng.0c09413
ACS Sustainable Chem. Eng. XXXX, XXX, XXX−XXX

Since the FFF 3DP is a high-temperature process, some changes in the polymer structure could be expected. However, no visible changes between FF_F and FF_P spectra were noted. According to Jia,[19] the bands in the region of 921 and 955 $cm^{-1}$ can be responsible for crystalline and amorphous phases of the PLA, respectively. In the case of FF_F, the intensity of the band at 955 $cm^{-1}$ (amorphous) matches well with the literature data.[19] This suggests the larger share of the amorphous state of PLA and indicates that the crystallization process as a result of the 3DP did not occur. The PLA/TPS filament showed a small "crystalline" band at 925 $cm^{-1}$, which slightly decreased after the printing process (Figure 4b). This might suggest that due to the fast cooling rate during FFF 3DP, the degree of the crystalline phase decreased slightly. There was also a slight decrease in the intensity of the −OH-derived signal in the PLA/TPS printout, which may be related to the reduction of hydrogen bonds as a result of the 3DP process. It is also worth noting that in the PLA/TPS_P spectrum, the band at ∼1652 $cm^{-1}$ appeared. This range corresponds to the presence of water molecules or C═C bond vibrations resulting from the decomposition of the material.[20] However, no changes in the intensity or positions of the main bands were noted; thus, it can be observed that the materials during the 3DP process were stable. Therefore, the signal at ∼1652 $cm^{-1}$ probably comes from the dampness of the material.

To expand chemical structure analysis of the filaments, the complementary technique, that is, Raman spectroscopy, was performed (Figure 5).

The obtained spectrum for the FF_F sample was generally in line with the FTIR results. Characteristic signals derived from PLA were noted: symmetric and asymmetric vibrations of −CH (2951 and 2887 $cm^{-1}$, respectively); the C═O carbonyl group (1774 $cm^{-1}$); $CH_3$ asymmetric modes (1453 $cm^{-1}$); C−O stretching (1045 $cm^{-1}$); C−COO vibration (874 $cm^{-1}$), and C═O stretching at 749 $cm^{-1}$.[19,21] Moreover, the presence of additional strong signals in regions characteristic for aromatic structures was also noted at 1532 and 690 $cm^{-1}$. Those additional signals come from the −CH stretching vibration of the aromatic ring (1532 $cm^{-1}$) and the bending vibration of the Ar ring (690 $cm^{-1}$), as Raman spectroscopy is relatively sensitive to these structures.[22,23] According to the information from the manufacturer, the FF, apart from PLA, contains additional substances, that is, TPE (4%) and mineral oils (up to 1%). Both additives contain aromatic carbons in their structure, which correspond to the additional signals located on the Raman spectrum. In turn, the Raman spectrum of PLA/TPS_F (Figure 5b) significantly complemented the characteristics of the composition. In addition to the PLA-derived bands, that is, C−H stretching (2954 and 2889 $cm^{-1}$); C═O stretching (1775 $cm^{-1}$); C−H bending (1458 $cm^{-1}$); C−O stretching (1042 $cm^{-1}$), and C−COO vibrations (878 $cm^{-1}$), the TPS-derived bands were noted. They corresponded to the peaks at 3010 $cm^{-1}$ (−OH stretching) and 1309 $cm^{-1}$ (C−O−H bending) as well as to the range of deformation modes in the glycoside bond present in the TPS structure (C−O, C−C, and C−O−C deformative vibrations in the range of 1088−1129 $cm^{-1}$).[18,24] However, when analyzing the spectroscopic results of both of the studied materials, no significant changes in the spectra of filaments and printouts were observed. There was no carbonyl peak splitting, which would indicate re-crystallization as a result of the printing process. Further, there were no visible bands shifts or changes in their intensity; hence, the structural stability of both studied materials under given printing conditions can be pre-confirmed.

For further structural analysis, both materials were studied by means of XRD (Figure 6).

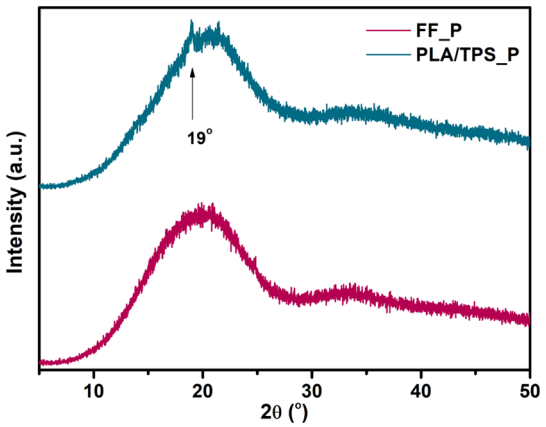


**Figure 6.** XRD spectra of FF_P and PLA/TPS_P.

The XRD analysis of FF_P showed a broad hump in the range of 2$\theta$ equal to 10−25°, which is characteristic for amorphous-based PLA.[21,25] This confirms the previous spectroscopic considerations that confirmed the amorphous nature of the studied FF. PLA/TPS_P showed a similar course with a slight peak at 2$\theta$ = 19°. According to Bulatović et al.,[26] TPS is formed by the process of plastification and destruction of the native starch crystalline structure; hence, the TPS shows a semi-crystalline-to-amorphous behavior. Thus, a slight peak at 2$\theta$ = 19° can correspond to residues of the A-type crystals present in the native starch.[27] Nevertheless, the mild course of the XRD plot and the lack of clear peaks corresponding to the crystal structure indicate a high proportion of the amorphous phase in both tested materials.

**Thermal and Thermomechanical Properties of the FF and PLA/TPS Filament and Printout.** Thermal characteristics of both materials before and after the printing process are presented in Figure 7. First, DSC measurements were performed. The results are shown in Figure 7a,b, and the corresponding numerical values are listed in Table 3. Based on the thermograms, the glass transition temperature region ($T_g$), cold crystallization ($T_{cc}$), crystalline phase transition ($T_{ct}$), melting temperature ($T_m$), heat of cold crystallization ($\Delta H_{cc}$), heat of melting ($\Delta H_m$), and degree of crystallinity ($X_c$) were determined.

The glass transition of polymers is a gradual phenomenon that takes place in a certain temperature range.[28,29] Although the so-called glass transition temperature (within the meaning of a single temperature value) is an incorrect concept, to facilitate comparison and analysis, Table 3 summarizes the single $T_g$ values corresponding to the midpoint of the heat capacity change recorded in DSC scans. The commercial FF_F PLA filament showed a $T_g$ at 67.4 °C, a $T_{cc}$ at 96.6 °C, a $T_{ct}$ at 156.3 °C, and a melting point at 171.9 °C. The calculated degree of crystallinity was 12.2%. The characteristic exothermic peak ($T_{ct}$) is associated with PLA polymorphism. These values are typical for PLA filaments and do not significantly differ from the literature data.[30] As a result of the FFF 3DP process (FF_P sample), a shift of the $T_g$ value (∼3 °C) toward lower temperatures was noted. This suggests a very slight increase in the mobility of the polymer chains in the amorphous state.

The glass transition, melting point, and degree of crystallinity for the PLA/TPS filament were found to be 70.8 °C, 165.2 °C,




https://doi.org/10.1021/acssuschemeng.0c09413
ACS Sustainable Chem. Eng. XXXX, XXX, XXX−XXX

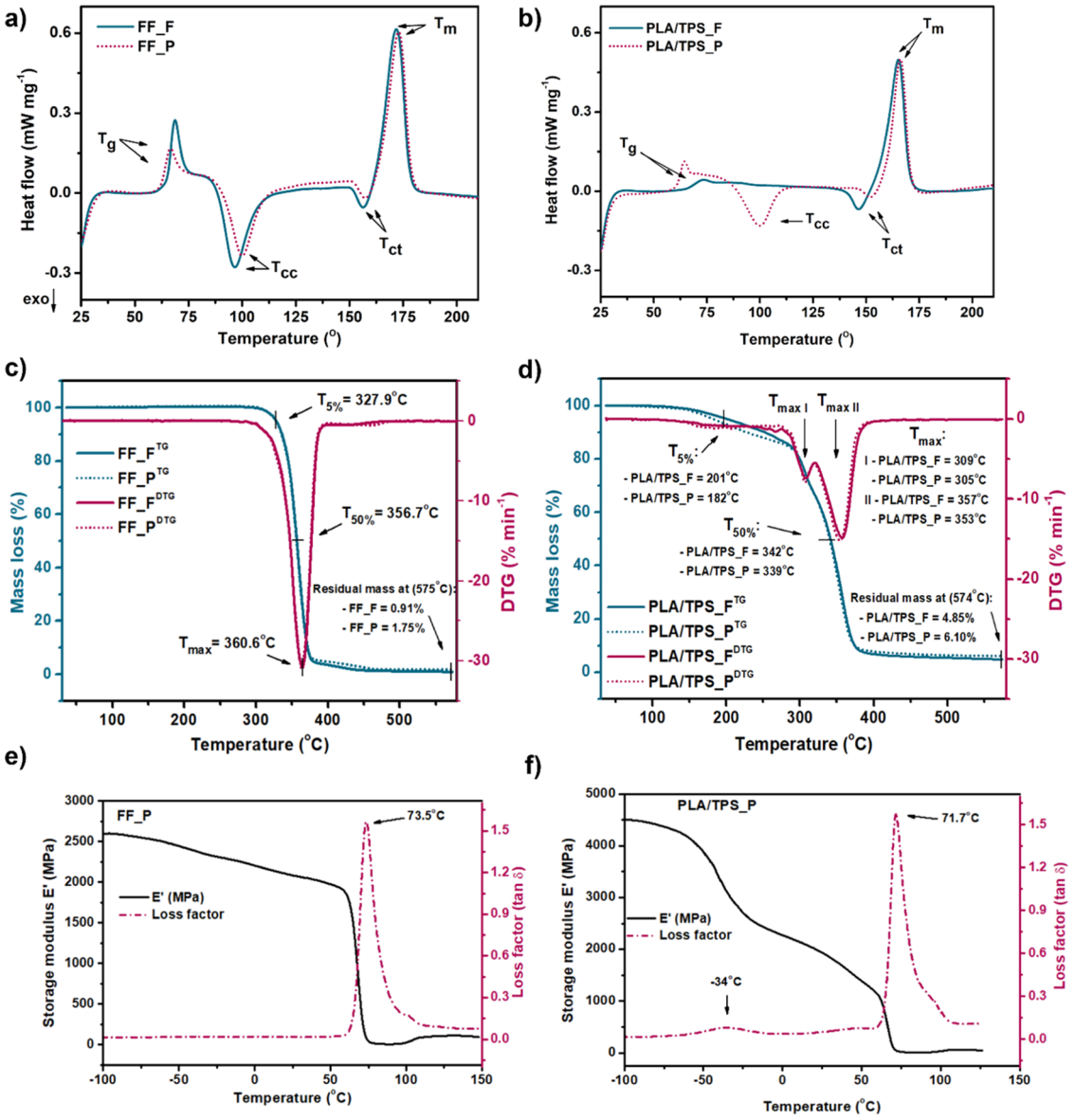


**Figure 7.** Thermal and thermomechanical characteristics of the FF and PLA/TPS filament and printout; (a,b) DSC curves (first heating run), (c,d) thermogravimetric curves TG and DTG, and (e,f) DMA results.

**Table 3. Values of DSC Measurements for the FF and PLA/TPS Filament and Printout (First Heating Run)**

| sample | $T_g$[a] (°C) | $T_{cc}$ (°C) | $\Delta H_{cc}$ (J g$^{-1}$) | $T_{ct}$ (°C) | $T_m$ (°C) | $\Delta H_m$ (J g$^{-1}$) | $X_{c\ PLA}$ (%) |
|---|---|---|---|---|---|---|---|
| FF_F | 67.4 | 96.6 | 22.3 | 156.3 | 171.9 | 33.1 | 12.2 |
| FF_P | 64.7 | 100 | 19.8 | 157.3 | 172.9 | 30.9 | 12.6 |
| PLA/TPS_F | 70.8 | | | 146.5 | 165.2 | 25.9 | 46.3 |
| PLA/TPS_P | 63.1 | 100 | 12.6 | 151.9 | 166.1 | 22.3 | 17.4 |

[a]The value provided in the table corresponds to the midpoint of the heat capacity change recorded in DSC scans.

and 46.3%, respectively. No cold crystallization process was found in the thermogram of the formed PLA/TPS filament (Figure 7b). This indicates sufficient cooling time during the filament-formation process to achieve a very high degree of crystallinity of the sample ($X_{c\ PLA}$ = 46.3%). The printed sample (PLA/TPS_P) showed a cold crystallization transformation at 100 °C during DSC analysis, which indicates that the cooling rate for the printout process was higher than the one for filament making. What is more, a significant reduction in the degree of crystallinity to 17.4% was observed. It follows that the 3DP process significantly affects the degree of crystallization of the PLA/TPS filament. Therefore, when planning a 3DP process with this filament as a feedstock, the above considerations should be taken into account. Moreover, the manufacturer can manipulate with a cooling rate or annealing after printing to achieve various values of crystallinity and thus different properties of the material. In this manner, by post-treatment (annealing), it is possible to obtain details with a relatively higher thermal resistance, hardness, or increased resistance to solvents.[31] Furthermore, a decrease of the $T_g$ by 7 °C relative to


https://doi.org/10.1021/acssuschemeng.0c09413
ACS Sustainable Chem. Eng. XXXX, XXX, XXX−XXX

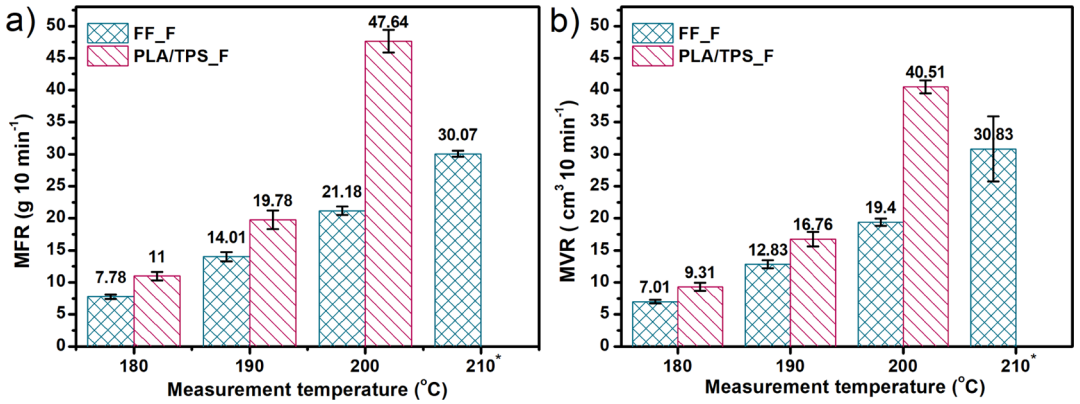


**Figure 8.** MFR (a) and MVR (b) results for the FF and PLA/TPS filament. The load was 2.16 kg. * At 210 °C, the melt fluidity of PLA/TPS_F was too high, and it was not possible to receive the data.

that of the PLA/TPS filament was also noted. Such a decrease in the glass transition temperature of the printed sample may be related to the destruction of hydrogen bonds occurring in the PLA/TPS structure and thus the increase in the mobility of the polymer chains. It is consistent with the FTIR results, which showed a clear decrease in the intensity of the −OH band of the PLA/TPS_P sample compared to that of PLA/TPS_F.

Subsequently, the thermal stability of both filaments and printouts was determined based on the TGA measurements. The curves show the amount and rate of change in the mass of a sample as a function of temperature. Obtained curves and their derivatives (DTG) are shown in Figure 7c,d. The thermograms of the commercial filament and printout indicated a single-stage degradation course, and their curves overlap to a large extent. The thermal stability ($T_{offset}$) of FF_F and FF_P was around 320 °C, while the complete decomposition takes place above 500 °C. There was no effect of the 3DP process on the course of the FF thermograms.

In turn, the thermal stability of PLA/TPS_F was ∼200 °C. The PLA/TPS material as a two-component composition showed a two-stage degradation course with distinctly separated DTG peaks (Figure 7d), thus confirming the polymer phase separation.[32] The first DGT peak ($T_{max\ I}$) for the PLA/TPS_F sample corresponds to the decomposition of TPS at 309 °C, while destruction of the PLA takes place at 357 °C ($T_{max\ II}$). The $T_{offset}$ for the PLA/TPS_P sample dropped by 19 °C, while the $T_{max\ I}$ and $T_{max\ II}$ dropped by 4 °C. The decrease in thermal stability was probably related to the dropped crystallinity degree of PLA/TPS_P observed after the 3DP process. Thus, unlike the FF_F, the thermal stability of the PLA/TPS filament is slightly changed due to the 3DP process. Moreover, the 3D printing temperature of PLA/TPS_F should not exceed ∼190 °C to avoid possible degradation and release of glycerin vapors originally contained in TPS ($T_{5\%}$ = 201 °C).

DMA results are presented in Figure 7e,f. The curves show the temperature dependence of storage modulus ($E'$) and loss factor (damping factor). As a standardized sample size is required for DMA measurements, the test was performed only for printed samples (FF_P and PLA/TPS_P). The maximum of the loss factor curves indicates the relaxation processes occurring near the glass transition temperature region of polymers[33] and was observed at 73.5 °C for FF_P and 71.7 °C for PLA/TPS_P. The value of $E'$ in the glassy state region of FF_P was above 2550 MPa and decreased rapidly after exceeding 65 °C (700 MPa). The maximum amplitude of the damping factor for FF_P reached 1.55 which corresponds to an impeccable damping property. The loss factor curve of PLA/TPS_P (Figure 7f) revealed the presence of an additional transition peak at −34 °C. It is most likely related to the $\alpha$-relaxation of the TPS molecules.[34,35] It can also be seen that FF_P is characterized by significantly higher values of the $E'$ over the entire temperature range than those for PLA/TPS_P and thereby exhibits greater stiffness.

Conducted thermal and thermo-mechanical studies showed a similar trend in thermal characteristics of both filaments. Moreover, the tests revealed that the 3DP process does not significantly affect the properties of the commercial filament. On the other hand, the printing process slightly changes the degree of crystallinity of the PLA/TPS_P sample, which results in a slight deterioration of the thermal stability of the PLA/TPS printouts. The two-phase nature of the prepared PLA/TPS composition was also confirmed. It has also been observed that due to the addition of TPS into PLA, the $T_m$ of the composition is lowered; thus, effectively, the temperature of 3D printing is reduced.

**MFR and MVR Results.** The MFR and MVR characterize the flow velocity of thermoplastics under thermal processing. These values express the number of grams or volumes of material pressed during 10 min through a die of a specific diameter under specific load and temperature. The MFR/MVR values are also inversely proportional to the dynamic viscosity of the melt as well as allow for a quick and easy way to estimate the appropriate printing temperature for the tested filament. Furthermore, according to Wang et al.,[36] the MFR/MVR is related to the inter-layer adhesion of details formed by FFF 3DP. Thus, it is worth paying attention to this study. The MFR/MVR results of commercial PLA (FF_F) and self-made PLA/TPS_F are presented in Figure 8.

The FF_F showed an MFR ranging from ∼8−30 g 10 min$^{-1}$ at 180 and 210 °C, respectively. The proportional increase in the index (by about 7 g 10 min$^{-1}$ per 10 °C) with the increasing measurement temperature was noted. This proves the high stability of the material and a wide range of effective plasticizing temperature and thus a comparatively wide range of possible 3DP temperatures. When compared to other commercial PLA filaments, the MFR value of the FF_F sample was relatively high. The PLA filament from Prusa (Prusament PLA) indicates that MFR = 10.4 g 10 min$^{-1}$ and that of Ultimaker PLA and Fiberlogy R-PLA around 6 g 10 min$^{-1}$ (at 210 °C, 2.16 kg). These values were over 3 times lower than those recorded for FF_F (MFR = 30 g 10 min$^{-1}$). This may be due to the lower molecular weight of FF PLA or the presence of additives (TPE and mineral oils)




https://doi.org/10.1021/acssuschemeng.0c09413
ACS Sustainable Chem. Eng. XXXX, XXX, XXX−XXX

**Table 4. Summarized Result of Mechanical Studies of FF_P and PLA/TPS_P**

| sample | print orientation | raster angle (deg) | Young modulus (GPa) | ultimate tensile strength (MPa) | elongation at break (%) | Charpy impact strength eU[a] (kJ m$^{-2}$) | hardness (Sh D) | brittleness (% Pa $10^{-10}$) |
|---|---|---|---|---|---|---|---|---|
| FF_P | *XY* | 0 | 1.62 ± 0.25 | 15.81 ± 5.19 | 2.97 ± 1.26 | 13.31 ± 1.47 | 79 ± 2 | 1.611 |
| | | 45 | 1.69 ± 0.31 | 15.21 ± 4.58 | 2.67 ± 0.46 | 9.00 ± 1.01 | 78 ± 3 | 1.792 |
| | | 90 | 1.597 ± 0.08 | 15.36 ± 3.05 | 1.83 ± 0.29 | 7.59 ± 1.33 | 78 ± 1 | 2.615 |
| | *ZX* | 0 | 2.03 ± 0.13 | 21.81 ± 3.36 | 4.28 ± 0.75 | 18.48 ± 1.63 | | 1.118 |
| | | 45 | 1.53 ± 0.22 | 5.83 ± 2.29 | 5.28 ± 0.55 | 15.84 ± 1.87 | | 0.906 |
| | | 90 | 2.19 ± 0.64 | 11.83 ± 3.06 | 3.68 ± 0.73 | 12.98 ± 0.88 | | 1.300 |
| PLA/TPS_P | *XY* | 0 | 1.47 ± 0.36 | 24.72 ± 1.21 | 3.83 ± 0.31 | 7.65 ± 0.94 | 60 ± 2 | 1.355 |
| | | 45 | 1.45 ± 0.37 | 9.35 ± 1.78 | 1.25 ± 0.12 | 4.97 ± 1.11 | 62 ± 2 | 4.152 |
| | | 90 | 1.93 ± 0.47 | 14.86 ± 1.42 | 3.11 ± 1.19 | 3.88 ± 1.31 | 61 ± 3 | 1.669 |
| | *ZX* | 0 | 1.51 ± 0.38 | 17.85 ± 1.31 | 4.61 ± 0.11 | 9.73 ± 1.04 | | 1.126 |
| | | 45 | 1.53 ± 0.35 | 17.28 ± 1.41 | 3.78 ± 0.52 | 5.91 ± 0.64 | | 1.373 |
| | | 90 | 1.74 ± 0.41 | 16.87 ± 2.15 | 2.57 ± 0.78 | 4.44 ± 0.91 | | 2.019 |

[a]eU—unnotched Charpy specimen.

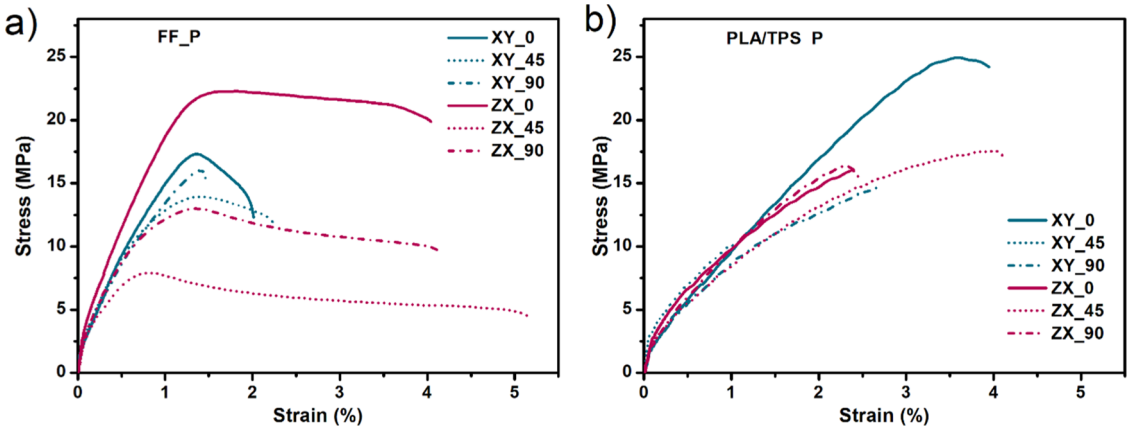


**Figure 9.** Average tensile stress−strain curves of FF_P (a) and PLA/TPS_P (b) depending on the build orientation and raster angle.

that act as PLA plasticizers, thus increasing MFRs under test conditions.

The MFR value of self-made PLA/TPS_F was in the range of 11 g 10 min$^{-1}$ at 180 °C to 47 g 10 min$^{-1}$ (200 °C). The rising trend of the index with the test temperature was much larger and more irregular compared to that of commercial FF_F. At 210 °C, the melt viscosity of PLA/TPS_F was too low to collect measurement data. In the temperature range of 200−210 °C, the initial material decomposition was recorded (color change and gas formation). Therefore, the 3DP temperature of the PLA/TPS filament should not exceed 200 °C. Due to the lack of research on the PLA filament modified with TPS in the literature, the discussion on PLA/TPS_F MFR values is difficult. However, considering the MFR threshold value for PLA filaments reported by Wang et al.[36] (∼10 g min$^{-1}$, at 2.16 kg), it can be concluded that the printing temperature for PLA/TPS_F at ∼180 °C is proper.

As the MFR increases, the melt fluidity becomes higher. Thus, it can be assumed that it is easier for the 3DP extruder to push the molten plastic through the die, and therefore, the printing speed can be higher. Nevertheless, it should be remembered that the high MFR may be also related to the low molecular weight of the polymer or its partial degradation under the measurement conditions, which can significantly deteriorate the print quality. Therefore, when analyzing the MFR of filaments for 3DP, one should also simultaneously consider the data derived from DSC and TGA.

**Effect of the Print Orientation and Raster Angle on Mechanical Properties (Tensile and Impact Strength and Brittleness).** Since there are no specific standards for testing the mechanical properties of FFF 3DP filaments so far, the tensile and impact strength tests were performed taking into account two types of print orientation (*XY* and *ZX*) and three values of raster angle (0, 45, and 90°). The results are summarized in Table 4.

The results of the tensile test of the FF_P samples in the *XY* configuration showed no visible dependence on the raster angle. The Young modulus was in the range of 1.6−1.7 GPa, the tensile strength was around 15−16 MPa, and the elongation at break was at 1.8−3.0%. It was noticed that in the *ZX* orientation, the FF_P samples showed higher strength parameters than that in *XY*, in particular, the Young modulus and elongation at break (∼22 GPa and 4.5%, respectively). Furthermore, the Charpy impact strength of FF_P_*ZX* samples was significantly higher than that of FF_P_*XY*. In turn, considering the raster angle, it was observed that the FF_P_0° system showed the highest overall strength parameters, while the FF_P_90° system exhibited the lowest impact strength (∼7.6 kJ m$^{-2}$) and the FF_P_45° system had the lower tensile strength.

For the PLA/TPS system, again the samples printed at a raster angle of 90° showed the lowest impact strength; in turn, *ZX*_0° had the highest values of elongation at break (4.6%) as well as tensile (17.8 MPa) and impact strengths (9.7 kJ m$^{-2}$). However, the Young modulus in both print orientations (*XY* and *ZX*) was





https://doi.org/10.1021/acssuschemeng.0c09413
ACS Sustainable Chem. Eng. XXXX, XXX, XXX−XXX

the highest for the 90° raster angle. In the case of PLA/TPS material, it is difficult to clearly determine which orientation of the printout (*XY* and *ZX*) shows the most favorable values.

As FFF printouts cannot be treated as a continuous material (isotropic material),[37] the assessment of the mechanical properties of such products is difficult. The stress−strain curves of FF_P and PLA/TPS_P are presented in Figure 9. It should be noted that the course of the FF_P curves more closely resembles those of ductile materials than that of PLA/TPS_P. Here,[13] we noticed that the addition of the TPS composition to pure PLA increases the elongation at break while lowering the tensile strength. However, these studies were carried out on injected-molded (continuous) test samples. Thus, it can be assumed that due to insufficient interlayer adhesion of FFF 3D-printed specimens, the effect of increased ductility of PLA/TPS_P samples was not observed.[37]

Summarizing, for both studied filaments, the *ZX*_0° configuration showed the most favorable strength parameters. Similar observations were reported by Chacón et al.[38] In the article, the influence of a number of FFF 3DP parameters on the mechanical properties of PLA was investigated. It was found that the on-edge (*ZX*) print orientation exhibits the most optimal mechanical properties in terms of strength, stiffness, and ductility. However, studies conducted by Dave et al.[39] have shown that the flat orientation (*XY*) of PLA printouts possesses the highest tensile strength. The presented discrepancies indicate the need to take into account additional printing conditions (layer height, flow rate, print speed, temperature conditions, etc.) when comparing the mechanical properties of resulting printouts.[40] Thus, it is highly desirable to standardize methods of assessing the mechanical properties of details obtained with FFF 3DP in order to be able to effectively test and compare new filaments.[37]

Generally, the concept of material brittleness is recognized indirectly—not quantitatively, for example, by evaluation of the results of the tensile test. It is related to the analysis of the fracture surface type or the character of the stress−strain curve. However, these methods constitute a qualitative analysis—they only provide information on whether the material is brittle- or ductile-type. Recently, Brostow et al.[17] proposed an equation that allows for quantitative validation of the material's brittleness. According to this definition, the brittleness ($B$) is inversely proportional to the product of tensile elongation at break ($\varepsilon_b$) and storage modulus ($E'$). Thus, when these values increase, the value of $B$ decreases. In our considerations, the storage modulus value is constant for each of the tested materials and equal to 2090 MPa for FF and 1927 MPa for PLA/TPS (data were taken from Figure 7e,f at 25 °C), while the $\varepsilon_b$ parameter is variable and depends on the printout configuration (as shown in Table 4). Thus, the samples with the highest $\varepsilon_b$ trend are predicted to be the least brittle ($B$ = 0.906 for FF_*ZX*_45° and $B$ = 1.126 for PLA/TPS_*ZX*_0°). However, comparing these materials to others tested by[41] the obtained value of $B$, which is in the range of around 1.0−4.0 (see Table 4), suggests rather high brittle properties. For comparison, Hytrel (TPE which represents ductile-type materials with a very high elongation at break) exhibits a brittleness ($B$) of less than 0.1, whereas unmodified polystyrene (known as a brittle-type polymer) has a value of around 9.0.[41]

**Effect of Infill Density on Compression Strength.** The uniaxial compression test was another study aimed at characterizing the mechanical properties of FF_P and PLA/TPS_P. Samples with three different infill densities were studied (25, 50, and 100%), and the results are displayed in Table 5.

**Table 5. Results of the Compression Test for FF_P and PLA/TPS_P Samples**

| infill density | 25% | 50% | 100% |
|---|---|---|---|
| | yield strength (MPa) | | |
| FF_P | 20.44 ± 0.63 | 34.64 ± 4.77 | 82.49 ± 8.32 |
| | compression strength (MPa) | | |
| PLA/TPS_P | 9.44 ± 2.53 | 19.65 ± 3.83 | 30.13 ± 0.91 |

The compressive strength of the printouts increases with the increase in the degree of infill.[42] This effect is more visible for the FF_P samples where a more than 4-fold increase in the yield strength was noted. For PLA/TPS_P, the increase in compressive strength was proportional to the increase in the infill density, reaching a value of ∼30 MPa (100% infill).

The course of the compression curves is presented in Figure 10. The stress−strain curves of the FF_P samples showed a clear yield point (*), while for PLA/TPS_P, the course is mild and characteristic for elastic polymers (Figure 10b). Therefore, for PLA/TPS_P samples, the inflection point of the curves (marked as #) was adopted as the compressive strength.

**Water Contact Angle.** During the measurement of the contact angle, significant changes in the wettability values were noticed depending on the direction of the sample arrangement on the measuring table and thus the sample's raster angle. Changing the raster angle to 90° significantly increased the hydrophobicity of both samples. The wCA of FF_P was ∼75 for 0° raster angle and around 111 for 90° raster angle, which correspond to the moderately hydrophilic to hydrophobic surface nature (Table 6). PLA/TPS_P showed a more hydrophilic surface with the wCA ranging from 63 to 81°. The difference in wettability between FF_P and PLA/TPS_P is related to the presence of TPS, which, being a highly hydrophilic material, lowers the contact angle of PLA.[43] However, such large differences in the wCA depending on the raster angle should be considered in terms of surface morphology and not of the material properties.

According to the literature, PLA shows poor hydrophilicity in the range 70−95° of the static wCA.[44] However, these values refer to a solid PLA surface (continuous material, most commonly obtained by plastic molding) and not to FFF 3DP printouts, which are characterized by many defects (voids) and discontinuities in the structure.[45]

The surface of the FFF 3DP samples consists of connected layers of polymer fibers of a given thickness and height. As a result, the printed surface (on a micro-scale) is wavy. Thus, due to the unevenness of the surface, the applied drop of water wets the material depending on the direction of the fibers on which it is placed, which radically changes the contact angle. The above considerations are confirmed by the Modi and Prakash[46] study, in which they proved that the orientation and raster angle of the FFF 3D-printed parts significantly affect the wettability of PLA. They found huge differences in the values of the PLA wCA, ranging from 40 to 75° for 0 and 90° raster angles, respectively.

Therefore, we believe that the standard method of contact angle measurement does not provide reliable data. The influence of the surface shape on the wCA should be minimized by significantly reducing the measuring droplet. Otherwise, the sample's data regarding the printing parameters and printout





https://doi.org/10.1021/acssuschemeng.0c09413
ACS Sustainable Chem. Eng. XXXX, XXX, XXX−XXX

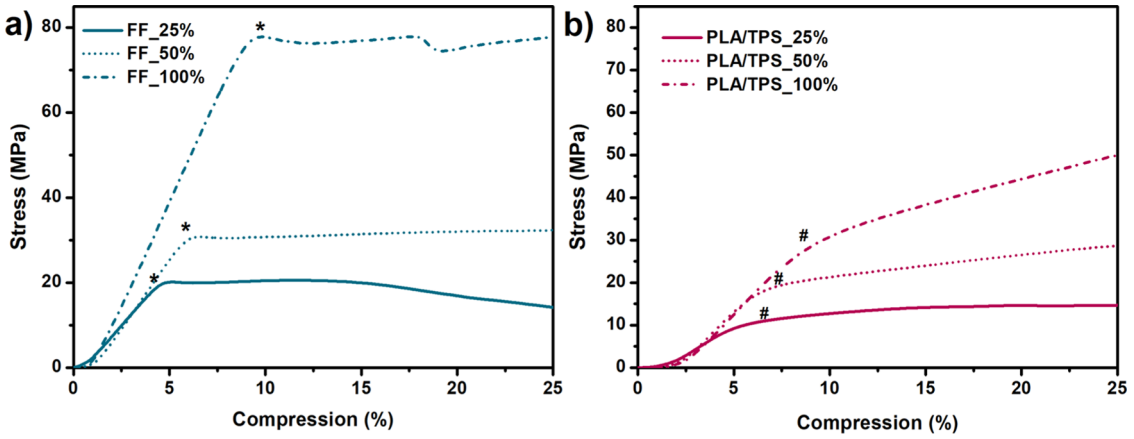


**Figure 10.** Averaged compressive stress−strain curves of FF_P (a) and PLA/TPS_P (b) depending on the infill density. * Yield strength; # compression strength.

**Table 6. CAs of FF_P and PLA/TPS_P with Different Raster Angles (0 and 90°)**

| Sample | FF_P | | PLA/TPS_P | |
|---|---|---|---|---|
| Raster angle | 0° | 90° | 0° | 90° |
| wCA (°) | 75.77 ± 4.35 | 111.46 ± 4.29 | 63.03 ± 1.79 | 81.54 ± 2.43 |

design should be precisely specified to allow the reliable comparison of the printout surface properties.

**Incubation of the Filaments in 0.1 PBS Solution and Canola Oil (Mass Loss, Swelling, and pH Measurements).** PLA, as a representative of biodegradable polymers, undergoes hydrolytic degradation in the PBS environment, which might proceed through the surface or bulk erosion mechanism.[47] However, in the case of solid PLA with a relatively high molecular weight (so-called injection or extrusion grades), the PBS degradation might proceed up to 5 years.[48] Therefore, PLA belongs to the long-term degrading biopolymers. Besides temperature, pH, and molecular weight, the ability of water to diffuse into the PLA matrix is the main factor that controls the degradation process.[47] Consequently, to estimate the degradability of both filaments, the incubation in 0.1 M PBS solution at 37 °C for 30 days was performed. During the PBS incubation, the weight change, the pH of the solution, and SEM images were recorded. Figure 11a,b represents the mass loss of the samples and the pH change of the PBS buffer with respect to the immersion time for FF_F and PLA/TPS_F, respectively.

The recorded change in the weight of the FF filament during 30 days of PBS incubation not exceeding 0.1%, as well as the relatively constant pH (7.50−7.48), indicates the stability of the material under given conditions. This is confirmed by SEM photos, which show no changes in the morphology of the surface or the cross-section of FF_F (Figure S3). This is in line with other studies of PLA degradation in the PBS medium, in which no mass changes or drops in pH were recorded during the 56 days of study.[49]

In turn, during the incubation of the PLA/TPS filament in PBS, significant changes in both mass and pH were noted. Thermoplastic starch, as a material sensitive to water, enhances significantly the degradation process of the PLA/TPS filament. The mean mass loss after the first hour was 1.3%, and after 3 days, it increased sharply to 13%. At the end of the study, a mass loss of 14.5% was noted. At the same time, a drop in pH was observed, down to 7.38 after 3 days and 7.27 after 30 days of incubation. The acidification of the electrolyte could be related to material hydrolysis which results in oligomer and monomer formation.[50] The resulting PLA-carboxyl end groups,[51] as well as TPS-origin glucose, glycerin, or ESO, could lower the pH due to the dissociation in the PBS solution. The SEM images (Figure S3) of the PLA-TPS_F surface after 30 days of incubation show numerous cracks and discontinuities in the structure (red arrows), while the cross-view shows the formation of a fibrous-like structure that may have arisen as a result of washing out of the TPS particles from the PLA matrix. The resulting surface defects of the PLA/TPS structure may additionally facilitate the diffusion of water in the inner part of the filament, and thus increase the susceptibility to degradation of PLA itself.[52] Such an effect is highly desirable as we consider the developed filament to be biodegradable.

To confirm the above considerations, the FTIR spectra of the filament samples before (0 d) and after 30 days (PBS_30d) of PBS incubation were compared (Figure 11e,f). In the case of FF_PBS_30d, the spectrum did not change significantly. There was a slight decrease in the intensity of the band derived from the C═O group (1748 $cm^{-1}$), while the rest of the spectrum remained intact. The degradation of PLA/TPS_F proceeded mostly through the destruction of bonds originating from TPS (−OH 3310 $cm^{-1}$, −C−O 1020 $cm^{-1}$, and −COH 1080 $cm^{-1}$). The PLA-origin aliphatic $CH_2$ and ester groups (C═O 1747 $cm^{-1}$) were also broken. Thus, it can be assumed that the erosion of TPS and the resulting surface roughness, cracks, and voids promote hydration and thus facilitate degradation of PLA.





https://doi.org/10.1021/acssuschemeng.0c09413
ACS Sustainable Chem. Eng. XXXX, XXX, XXX−XXX

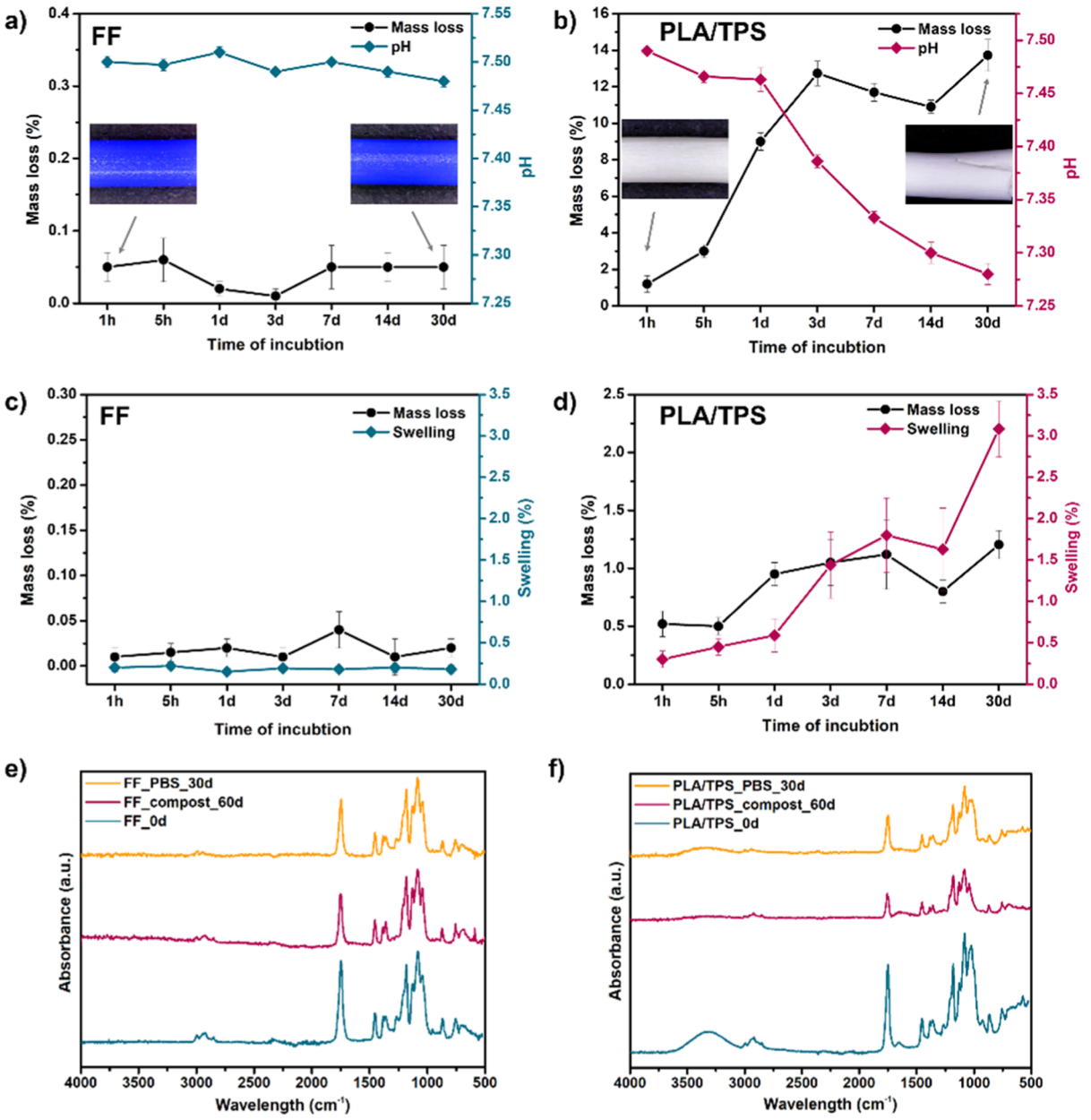


**Figure 11.** Results of degradation studies in 0.1 M PBS solution of (a) FF_F and (b) PLA/TPS_F. SEM images showing the process of PBS incubation are presented in the Supporting Information (Figure S3). The results of incubation in canola oil of (c) FF_F and (d) PLA/TPS_F. FTIR spectra of (e) FF_F and (f) PLA/TPS_F after 30 days of incubation in PBS and 60 days of composting.

For further characterization of studied filaments, the mass loss and swelling in contact with food-grade canola oil was investigated (Figure 11c,d). As expected, the FF filament showed high resistance to oil. Both the weight loss and the swelling ratio of the samples were unnoticeable, whereas the PLA/TPS_F swelling was ~3% and the weight loss was 1.2% after 30 days of testing. Thus, PLA/TPS_F shows moderate resistance to oil contact.

**Results of Laboratory-Scale Composting.** The laboratory composting study was conducted to assess the filament's susceptibility to disintegration in composting conditions. It should be noted that this study cannot be regarded as an assessment of the biodegradability of the bioplastic.[53] According to the EN 13432 standard, bioplastics marked as compostable should show a disintegration of 90% (into pieces smaller than a sieve with 2 mm of the mesh) over 90 days at 58 °C in the simulated compost.

Figure 12 shows the results of the composting test of FF and PLA/TPS 3D printouts. FF_P samples exhibited high composting resistance. There was no change in the weight during the test (Figure 12a), and the morphology of the samples was not intact. The discoloration of the samples was observed from about the 30th day of composting (Figure 12b). The surface of the sample remained homogeneous and smooth (Figure 12c) up to the 50th day of the study. Single surface cracks were recorded only after 60 days (Figure S4). However, the recorded FTIR spectrum of the sample after 60 days of the test (Figure 11e, FF_compost_60d) showed a noticeable decrease in the intensity of the bands, resulting from the vibration of the C═O (stretching at 1748 $cm^{-1}$ and bending at 1264 $cm^{-1}$) and C−O (stretching at 1043 $cm^{-1}$) bonds was




https://doi.org/10.1021/acssuschemeng.0c09413
ACS Sustainable Chem. Eng. XXXX, XXX, XXX−XXX

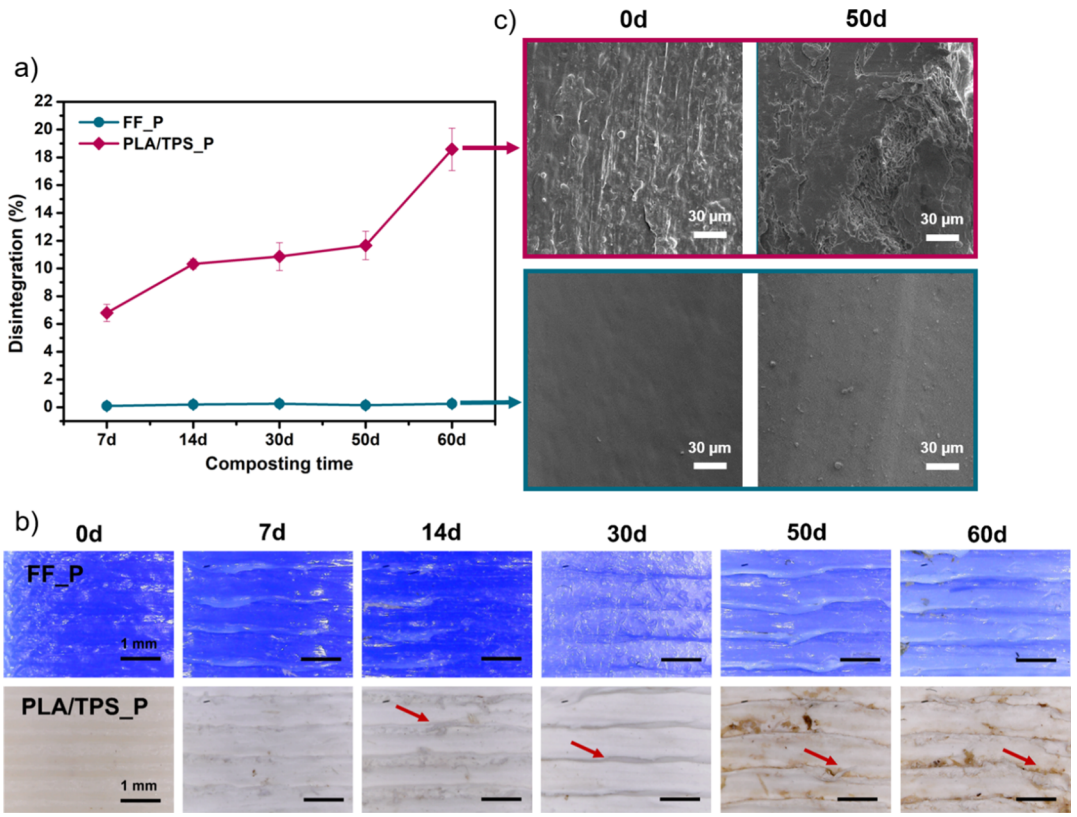


**Figure 12.** Results of a laboratory-scale composting test of FF_P and PLA/TPS_P: (a) disintegration degree over composting time, (b) optical microscopy images of samples before (0 d) and after 7, 14, 30, 50, and 60 days of composting (red arrows indicate progressive cracks and discontinuities of the PLA/TPS sample surface), and (c) representative SEM micrographs of the sample surface before (0 d) and after 50 days of composting (more SEM images are presented in the Supporting Information; Figures S4 and S5).

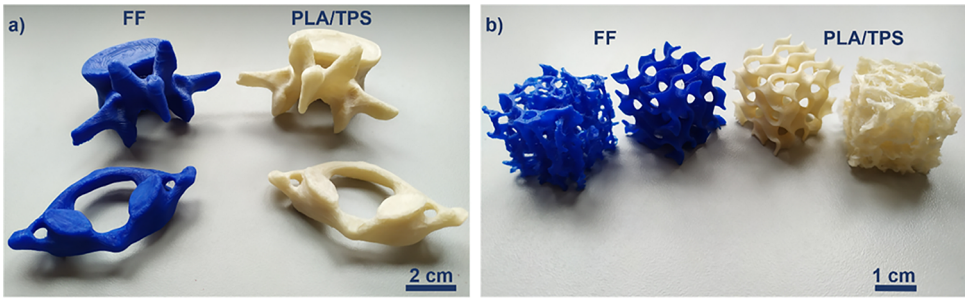


**Figure 13.** FFF 3D-printed FF and PLA/TPS complex structures: (a) personalized anatomical models of vertebrae C1 (atlas) and L3, (b) porous gyroid, and cancellous bone-like structure printouts. Detailed information on models and the 3DP process is presented in the Supporting Information (Figure S2 and Tables S2 and S3). More optical photos of the printouts can be found in Figure S6.

observed, which may indicate the initial destruction of the surface layer of the FF_P printouts. Nevertheless, overall, the FF_P was left practically intact under the 60 days of simulated composting. In turn, PLA/TPS_P showed an evident trend of an increased degree of disintegration during the composting time. Already after 7 days of incubation, a disintegration degree of 7% was noted, and at the end of the study, it reached over 18% (Figure 12a). Optical microscopy images showed the formation of cracks and defects on the sample's surface from the 14th day of testing. SEM micrographs revealed a high roughness and heterogeneity of the PLA/TPS_P surface compared to that of FF_P. At the beginning of composting, the TPS cavities were observed (14th day), where pinholes in the PLA/TPS_P structures were formed (Figure S5). The initially changed surface started to erode, and the destruction proceeded deeper into the structure, thereby destroying the sample in its entire volume. The FTIR spectrum confirms the above considerations (Figure 11f). There was a clear degradation of bonds originating mainly from TPS. Signals from vibrations of −OH (3310 $cm^{-1}$) and C−O groups (a glucose ring at 1020 $cm^{-1}$) were flattened, and the intensity of the whole spectrum significantly decreased. Therefore, the addition of TPS contributed to an increase in the susceptibility to the disintegration of PLA under composting conditions. This is most likely related to the facilitated penetration of moisture into the material and the presence of glucose (as a result of TPS degradation), which acts as a nutrient medium for the microorganisms present in the compost.[52]

The results of laboratory composting presented by Arrieta et al.[54,55] shows a disintegration rate of PLA of over 90% within 35 days. In turn, the study by Quiles-Carrillo et al.[56] conducted at




https://doi.org/10.1021/acssuschemeng.0c09413
ACS Sustainable Chem. Eng. XXXX, XXX, XXX−XXX

the same conditions (ISO 20200) reveals a disintegration of the PLA/TPS (40 wt % TPS) blend of over 90% after 57 days of composting. However, it should be noted that the above data refer to samples in the form of thin films with thicknesses of 0.1 and 1 mm, respectively. Therefore, it is difficult to compare these results with the values obtained for solid FF and PLA/TPS printouts. However, the findings of our earlier studies on the PLA/TPS/ESO composition (which was used to form the PLA/TPS filament) revealed that this material was completely disintegrated after 57 days of simulated composting[13] (the study was carried out on thin sheets with 2 mm thickness).

**Printability Assessment—FFF 3D Printing of Anatomical Models and Porous Structures.** Finally, to illustrate the usefulness of the developed PLA/TPS filament, complex-shaped details were printed and compared with those obtained from the commercial filament. The resulting printouts are presented in Figure 13. To allow a fair comparison of the printability of both filaments, they were printed with the same 3D printing settings. The only difference was the printing temperature, which was 215 °C for the FF_F and 185 °C for the PLA/TPS filament.

First, the personalized STL files of two types of vertebrae were converted from an abdominal CT scan. The scheme illustrating the process of segmentation and conversion is illustrated in Figure S2 (the Supporting Information). Thus, obtained projects required the use of support structures to ensure a good quality of printouts; hence, detachable-type supports were introduced. The printing process in both cases ran smoothly, and the printing times were ∼5.5 and 2 h for L3 and C1 vertebrae, respectively. As a result, personalized anatomical models with high surface mapping and quality and good dimensional stability were obtained. No shrinkage effect was noticed. Printouts with the PLA/TPS filament did not differ in quality in any way from those obtained from FF_F. Similar observations were made in the case of 3D printing porous structures (which were printed without the use of support structures). The gyroid project was very well mapped. No defects or discontinuities in the structure were observed for both the FF and PLA/TPS gyroid printouts (Figure 13b). Nevertheless, some issues were encountered in cancellous bone-like printouts. As this sponge-like structure possesses many overhangs and very thin walls, it is highly demanding for FFF 3D printing. The printout from the FF filament turned out to be defectless. In turn, in the case of PLA/TPS, some defects of the printout surface were noted. Pores of the cancellous bone-like structure were partially blocked by the so-called stringing, that is, thin threads made of the material leaking out of the printing nozzle (hotend) in an uncontrolled manner. However, this phenomenon can be minimized by changing the printing parameters such as speed, temperature, or the retraction distance. More challenges faced during 3DP with the PLA/TPS filament are described in Table S5 (the Supporting Information).

Summarizing, we can state that our developed bio-filament is suitable for effective FFF 3DP, and the printouts thus formed do not differ in quality from those obtained using available commercial filaments.

## CONCLUSIONS

In this work, we presented an extensive characteristic of a self-made bio-filament for FFF 3DP, consisting of PLA modified with TPS. For comparative purposes, the properties and printability of the PLA/TPS filament were confronted with those of the FlashForge PLA filament—the commercially available FFF filament. Our approach, namely, replacing up to 40% of PLA with TPS, resulted in considerable improvement of hydrophilicity, susceptibility to hydrolytic degradation, and thus enhancement of compostability in contrast to that of commercial PLA printouts. Furthermore, we demonstrated that the PLA/TPS filament shows a comparable printability to its commercial counterpart and is suitable for FFF 3DP of both personalized anatomical models as well as complex porous structures. We also believe that the developed filament might challenge traditional petroleum-based filaments as a more environmentally friendly alternative.

Furthermore, our results challenge/question commercial terms of marking filaments (e.g., PLA) as "biodegradable/eco-friendly". The use of a biopolymer as a base material cannot determine its final "bio-properties". The addition of printability-improving agents (oils and plasticizers) or fillers and pigments, at the stage of filament formation, may cause numerous changes in the pristine properties of the biopolymer (including a decrease in biodegradability). Due to that, the final product cannot be recognized as "eco-friendly", although it is based on biodegradable polymers. Therefore, to verify the filament's "eco-friendly" character, additional research should be carried out to establish whether a final product is truly biodegradable or it is only partly bio-based.

## ASSOCIATED CONTENT

### Supporting Information

The Supporting Information is available free of charge at https://pubs.acs.org/doi/10.1021/acssuschemeng.0c09413.

> Test sample preparation; preparation and description of the virtual models; SEM images of the degradation study in 0.1 M PBS; laboratory composting—compost composition and SEM images; images of printed anatomical models and porous structures; and description of challenges faced during 3D printing with the PLA/TPS filament (PDF)

## AUTHOR INFORMATION


### Corresponding Author

**Agnieszka Haryńska** − *Department of Polymers Technology, Faculty of Chemistry, Gdansk University of Technology (GUT), 80-233 Gdansk, Poland;* orcid.org/0000-0001-8017-6070; Email: agnieszka.harynska@pg.edu.pl

### Authors

**Helena Janik** − *Department of Polymers Technology, Faculty of Chemistry, Gdansk University of Technology (GUT), 80-233 Gdansk, Poland*

**Maciej Sienkiewicz** − *Department of Polymers Technology, Faculty of Chemistry, Gdansk University of Technology (GUT), 80-233 Gdansk, Poland*

**Barbara Mikolaszek** − *Department of Pharmaceutical Technology, Faculty of Pharmacy, Medical University of Gdansk, 80-416 Gdansk, Poland;* orcid.org/0000-0001-5894-7705

**Justyna Kucińska-Lipka** − *Department of Polymers Technology, Faculty of Chemistry, Gdansk University of Technology (GUT), 80-233 Gdansk, Poland*

Complete contact information is available at: https://pubs.acs.org/10.1021/acssuschemeng.0c09413






https://doi.org/10.1021/acssuschemeng.0c09413
ACS Sustainable Chem. Eng. XXXX, XXX, XXX−XXX

### Author Contributions

A.H. conceptualization, methodology, software, validation, investigation, writing—original draft, writing—review and editing, visualization, project administration. H.J. conceptualization, resources, writing—review and editing. M.S. material conceptualization, writing—review and editing. B.M. investigation (SEM), writing—review and editing. J.K.-L. resources, writing—review and editing.

### Funding

Part of the research realized at the Gdansk University of Technology (GUT) was financed by the Ministry of National Education via the Knowledge & Technology Transfer Center at the GUT under the program Innovation Incubator Plus.

### Notes

The authors declare no competing financial interest.

The raw data required to reproduce these findings cannot be shared at this time due to technical or time limitations. Nevertheless, they can be made available on request.

## ■ ACKNOWLEDGMENTS

We acknowledge Paulina Kosmela for technical help in conducting DSC, TGA, and DMA studies.

## ■ REFERENCES

(1) Wickramasinghe, S.; Do, T.; Tran, P. FDM-Based 3D Printing of Polymer and Associated Composite: A Review on Mechanical Properties, Defects and Treatments. *Polymers* **2020**, *12*, 1529.

(2) Sanchez-Rexach, E.; Johnston, T. G.; Jehanno, C.; Sardon, H.; Nelson, A. Sustainable Materials and Chemical Processes for Additive Manufacturing. *Chem. Mater.* **2020**, *32*, 7105−7119.

(3) Filgueira, D.; Holmen, S.; Melbø, J. K.; Moldes, D.; Echtermeyer, A. T.; Chinga-Carrasco, G. Enzymatic-Assisted Modification of Thermomechanical Pulp Fibers to Improve the Interfacial Adhesion with Poly(Lactic Acid) for 3D Printing. *ACS Sustainable Chem. Eng.* **2017**, *5*, 9338−9346.

(4) Song, X.; He, W.; Yang, S.; Huang, G.; Yang, T. Fused Deposition Modeling of Poly (Lactic Acid)/Walnut Shell Biocomposite Filaments-Surface Treatment and Properties. *Appl. Sci.* **2019**, *9*, 4892.

(5) Chang, Y.-C.; Chen, Y.; Ning, J.; Hao, C.; Rock, M.; Amer, M.; Feng, S.; Falahati, M.; Wang, L.-J.; Chen, R. K.; Zhang, J.; Ding, J.-L.; Li, L. No Such Thing as Trash: A 3D-Printable Polymer Composite Composed of Oil-Extracted Spent Coffee Grounds and Polylactic Acid with Enhanced Impact Toughness. *ACS Sustainable Chem. Eng.* **2019**, *7*, 15304−15310.

(6) Idrees, M.; Jeelani, S.; Rangari, V. Three-Dimensional-Printed Sustainable Biochar-Recycled PET Composites. *ACS Sustainable Chem. Eng.* **2018**, *6*, 13940−13948.

(7) Herrero, M.; Peng, F.; Núñez Carrero, K. C.; Merino, J. C.; Vogt, B. D. Renewable Nanocomposites for Additive Manufacturing Using Fused Filament Fabrication. *ACS Sustainable Chem. Eng.* **2018**, *6*, 12393−12402.

(8) Giubilini, A.; Siqueira, G.; Clemens, F. J.; Sciancalepore, C.; Messori, M.; Nystrom, G.; Bondioli, F. 3D Printing Nanocellulose-Poly(3-Hydroxybutyrate-Co-3-Hydroxyhexanoate) Biodegradable Composites by Fused Deposition Modeling. *ACS Sustainable Chem. Eng.* **2020**, *8*, 27.

(9) Kuo, C.-C.; Liu, L.-C.; Teng, W.-F.; Chang, H.-Y.; Chien, F.-M.; Liao, S.-J.; Kuo, W.-F.; Chen, C.-M. Preparation of Starch/Acrylonitrile-Butadiene-Styrene Copolymers (ABS) Biomass Alloys and Their Feasible Evaluation for 3D Printing Applications. *Composites, Part B* **2016**, *86*, 36−39.

(10) Ou-Yang, Q.; Guo, B.; Xu, J. Preparation and Characterization of Poly(Butylene Succinate)/Polylactide Blends for Fused Deposition Modeling 3D Printing. *ACS Omega* **2018**, *3*, 14309−14317.

(11) Andrzejewski, J.; Cheng, J.; Anstey, A.; Mohanty, A. K.; Misra, M. Development of Toughened Blends of Poly(Lactic Acid) and Poly(Butylene Adipate- Co-Terephthalate) for 3D Printing Applications: Compatibilization Methods and Material Performance Evaluation. *ACS Sustainable Chem. Eng.* **2020**, *8*, 6576−6589.

(12) Tanabe, I. Double-ECO Model Technologies for an Environmentally-Friendly Manufacturing. *Procedia CIRP* **2016**, *48*, 495−501.

(13) Przybytek, A.; Sienkiewicz, M.; Kucińska-Lipka, J.; Janik, H. Preparation and Characterization of Biodegradable and Compostable PLA/TPS/ESO Compositions. *Ind. Crops Prod.* **2018**, *122*, 375.

(14) Haryńska, A.; Carayon, I.; Kosmela, P.; Brillowska-Dąbrowska, A.; Łapiński, M.; Kucińska-Lipka, J.; Janik, H. Processing of Polyester-Urethane Filament and Characterization of FFF 3D Printed Elastic Porous Structures with Potential in Cancellous Bone Tissue Engineering. *Materials* **2020**, *13*, 4457.

(15) Kikinis, R.; Pieper, S. D.; Vosburgh, K. G. 3D Slicer: A Platform for Subject-Specific Image Analysis, Visualization, and Clinical Support. In *Intraoperative Imaging and Image-Guided Therapy*; Jolesz, F. A., Ed.; Springer New York: New York, NY, 2014; pp 277−289.

(16) Pyda, M.; Bopp, R. C.; Wunderlich, B. Heat Capacity of Poly(Lactic Acid). *J. Chem. Thermodyn.* **2004**, *36*, 731−742.

(17) Brostow, W.; Hagg Lobland, H. E.; Narkis, M. Sliding Wear, Viscoelasticity, and Brittleness of Polymers. *J. Mater. Res.* **2006**, *21*, 2422−2428.

(18) Nobrega, M. M.; Olivato, J. B.; Müller, C. M. O.; Yamashita, F. Biodegradable Starch-Based Films Containing Saturated Fatty Acids: Thermal, Infrared and Raman Spectroscopic Characterization. *Polimeros* **2012**, *22*, 475−480.

(19) Jia, W.; Luo, Y.; Yu, J.; Liu, B.; Hu, M.; Chai, L.; Wang, C. Effects of High-Repetition-Rate Femtosecond Laser Micromachining on the Physical and Chemical Properties of Polylactide (PLA). *Opt. Express* **2015**, *23*, 26932.

(20) Antończak, A. J.; Stępak, B. D.; Szustakiewicz, K.; Wójcik, M. R.; Abramski, K. M. Degradation of Poly(l-Lactide) under CO2 Laser Treatment above the Ablation Threshold. *Polym. Degrad. Stab.* **2014**, *109*, 97−105.

(21) Mallick, S.; Ahmad, Z.; Touati, F.; Bhadra, J.; Shakoor, R. A.; Al-Thani, N. J. PLA-TiO2 Nanocomposites: Thermal, Morphological, Structural, and Humidity Sensing Properties. *Ceram. Int.* **2018**, *44*, 16507−16513.

(22) Haryńska, A.; Carayon, I.; Kosmela, P.; Szeliski, K.; Łapiński, M.; Pokrywczyńska, M.; Kucińska-Lipka, J.; Janik, H. A Comprehensive Evaluation of Flexible FDM/FFF 3D Printing Filament as a Potential Material in Medical Application. *Eur. Polym. J.* **2020**, *138*, 109958.

(23) Schrader, B. Raman Spectroscopy of Mineral Oil Products. Part I: NIR/FT-Raman Spectra of Polycyclic Aromatic Hydrocarbons. *Appl. Spectrosc.* **1991**, *45*, 1230−1232.

(24) Peidayesh, H.; Ahmadi, Z.; Khonakdar, H. A.; Abdouss, M.; Chodák, I. Fabrication and Properties of Thermoplastic Starch/Montmorillonite Composite Using Dialdehyde Starch as a Crosslinker. *Polym. Int.* **2020**, *69*, 317−327.

(25) Tao, Y.; Shao, J.; Li, P.; Shi, S. Q. Application of a Thermoplastic Polyurethane/Polylactic Acid Composite Filament for 3D-Printed Personalized Orthosis. *Mater. Technol.* **2019**, *53*, 71−76.

(26) Bulatović, V. O.; Mandić, V.; Kučić Grgić, D.; Ivančić, A. Biodegradable Polymer Blends Based on Thermoplastic Starch. *J. Polym. Environ.* **2020**, *29*, 492.

(27) Teixeira, E. D. M.; De Campos, A.; Marconcini, J. M.; Bondancia, T. J.; Wood, D.; Klamczynski, A.; Mattoso, L. H. C.; Glenn, G. M. Starch/Fiber/Poly(Lactic Acid) Foam and Compressed Foam Composites. *RSC Adv.* **2014**, *4*, 6616−6623.

(28) Kalogeras, I. M.; Hagg Lobland, H. E. The Nature of the Glassy State: Structure and Glass Transitions. *J. Mater. Educ.* **2012**, *34*, 69−94.

(29) Kalogeras, I. M.; Brostow, W. Glass Transition Temperatures in Binary Polymer Blends. *J. Polym. Sci., Part B: Polym. Phys.* **2009**, *47*, 80−95.

(30) Matos, B. D. M.; Rocha, V.; da Silva, E. J.; Moro, F. H.; Bottene, A. C.; Ribeiro, C. A.; dos Santos Dias, D.; Antonio, S. G.; do Amaral, A. C.; Cruz, S. A.; de Oliveira Barud, H. G.; Silva Barud, H. d. Evaluation of Commercially Available Polylactic Acid (PLA) Filaments for 3D Printing Applications. *J. Therm. Anal. Calorim.* **2019**, *137*, 555−562.





https://doi.org/10.1021/acssuschemeng.0c09413
ACS Sustainable Chem. Eng. XXXX, XXX, XXX−XXX

(31) Benwood, C.; Anstey, A.; Andrzejewski, J.; Misra, M.; Mohanty, A. K. Improving the Impact Strength and Heat Resistance of 3D Printed Models: Structure, Property, and Processing Correlationships during Fused Deposition Modeling (FDM) of Poly(Lactic Acid). *ACS Omega* **2018**, *3*, 4400−4411.
(32) Turco, R.; Ortega-Toro, R.; Tesser, R.; Mallardo, S.; Collazo-Bigliardi, S.; Boix, A. C.; Malinconico, M.; Rippa, M.; Di Serio, M.; Santagata, G. Poly (Lactic Acid)/Thermoplastic Starch Films: Effect of Cardoon Seed Epoxidized Oil on Their Chemicophysical, Mechanical, and Barrier Properties. *Coatings* **2019**, *9*, 574.
(33) Menard, K. P. *Dynamic Mechanical Analysis: A Practical Introduction*, 2nd ed.; CRC Press, 2008.
(34) B, A.; Suin, S.; Khatua, B. B. Highly Exfoliated Eco-Friendly Thermoplastic Starch (TPS)/Poly (Lactic Acid)(PLA)/Clay Nanocomposites Using Unmodified Nanoclay. *Carbohydr. Polym.* **2014**, *110*, 430.
(35) Park, H.-M.; Li, X.; Jin, C.-Z.; Park, C.-Y.; Cho, W.-J.; Ha, C.-S. Preparation and Properties of Biodegradable Thermoplastic Starch/Clay Hybrids. *Macromol. Mater. Eng.* **2002**, *287*, 553−558.
(36) Wang, S.; Capoen, L.; D'hooge, D. R.; Cardon, L. Can the Melt Flow Index Be Used to Predict the Success of Fused Deposition Modelling of Commercial Poly(Lactic Acid) Filaments into 3D Printed Materials? *Plast., Rubber Compos.* **2018**, *47*, 9−16.
(37) García-Domínguez, A.; Claver, J.; Camacho, A. M.; Sebastián, M. A. Considerations on the Applicability of Test Methods for Mechanical Characterization of Materials Manufactured by FDM. *Materials* **2020**, *13*, 28.
(38) Chacón, J. M.; Caminero, M. A.; García-Plaza, E.; Núñez, P. J. Additive Manufacturing of PLA Structures Using Fused Deposition Modelling: Effect of Process Parameters on Mechanical Properties and Their Optimal Selection. *Mater. Des.* **2017**, *124*, 143−157.
(39) Dave, H. K.; Patadiya, N. H.; Prajapati, A. R.; Rajpurohit, S. R. Effect of Infill Pattern and Infill Density at Varying Part Orientation on Tensile Properties of Fused Deposition Modeling-Printed Poly-Lactic Acid Part. *Proc. Inst. Mech. Eng., Part C* **2019**, 1−17.
(40) Popescu, D.; Zapciu, A.; Amza, C.; Baciu, F.; Marinescu, R. FDM Process Parameters Influence over the Mechanical Properties of Polymer Specimens: A Review. *Polym. Test.* **2018**, *69*, 157−166.
(41) Brostow, W.; Hagg Lobland, H. E. Brittleness of Materials: Implications for Composites and a Relation to Impact Strength. *J. Mater. Sci.* **2010**, *45*, 242−250.
(42) Fadhil Alani, T.; Ali, H.; Abbas, D.; Mohammad Othman, D.; Basil Ali, H.; Author, C. Effect of Infill Parameter on Compression Property in FDM Process. *Int. J. Eng. Res. Appl.* **2017**, *7*, 16−19.
(43) Esmaeili, M.; Pircheraghi, G.; Bagheri, R.; Altstädt, V. Poly(Lactic Acid)/Coplasticized Thermoplastic Starch Blend: Effect of Plasticizer Migration on Rheological and Mechanical Properties. *Polym. Adv. Technol.* **2019**, *30*, 839−851.
(44) Biresaw, G.; Carriere, C. J. Correlation between Mechanical Adhesion and Interfacial Properties of Starch/Biodegradable Polyester Blends. *J. Polym. Sci., Part B: Polym. Phys.* **2001**, *39*, 920−930.
(45) Tronvoll, S. A.; Welo, T.; Elverum, C. W. The Effects of Voids on Structural Properties of Fused Deposition Modelled Parts: A Probabilistic Approach. *Int. J. Adv. Manuf. Technol.* **2018**, *97*, 3607−3618.
(46) Modi, U.; Prakash, S. Wettability of 3D Printed Polylactic Acid (PLA) Parts. *AIP Conf. Proc.* **2019**, *2148*, 030052.
(47) Elsawy, M. A.; Kim, K.-H.; Park, J.-W.; Deep, A. Hydrolytic Degradation of Polylactic Acid (PLA) and Its Composites. *Renew. Sustain. Energy Rev.* **2017**, *79*, 1346−1352.
(48) Saha, S. K.; Tsuji, H. Effects of Molecular Weight and Small Amounts of D-Lactide Units on Hydrolytic Degradation of Poly(l-Lactic Acid)S. *Polym. Degrad. Stab.* **2006**, *91*, 1665−1673.
(49) Chouzouri, G.; Xanthos, M. Degradation of Aliphatic Polyesters in the Presence of Inorganic Fillers. *J. Plast. Film Sheeting* **2007**, *23*, 19−36.
(50) Gorrasi, G.; Pantani, R. Hydrolysis and Biodegradation of Poly(Lactic Acid). *Advances in Polymer Science*; Springer New York LLC, 2018; Vol. *279*, pp 119−151.
(51) Chamas, A.; Moon, H.; Zheng, J.; Qiu, Y.; Tabassum, T.; Jang, J. H.; Abu-Omar, M.; Scott, S. L.; Suh, S. Degradation Rates of Plastics in the Environment. *ACS Sustainable Chem. Eng.* **2020**, *8*, 3494−3511.
(52) Rodrigues, C. A.; Tofanello, A.; Nantes, I. L.; Rosa, D. S. Biological Oxidative Mechanisms for Degradation of Poly(Lactic Acid) Blended with Thermoplastic Starch. *ACS Sustainable Chem. Eng.* **2015**, *3*, 2756−2766.
(53) Ruggero, F.; Gori, R.; Lubello, C. Methodologies to Assess Biodegradation of Bioplastics during Aerobic Composting and Anaerobic Digestion: A Review. *Waste Manage. Res.* **2019**, *37*, 959−975.
(54) Arrieta, M. P.; López, J.; Rayón, E.; Jiménez, A. Disintegrability under Composting Conditions of Plasticized PLA−PHB Blends. *Polym. Degrad. Stab.* **2014**, *108*, 307−318.
(55) Arrieta, M. P.; López, J.; Hernández, A.; Rayón, E. Ternary PLA-PHB-Limonene Blends Intended for Biodegradable Food Packaging Applications. *Eur. Polym. J.* **2014**, *50*, 255−270.
(56) Quiles-Carrillo, L.; Montanes, N.; Pineiro, F.; Jorda-Vilaplana, A.; Torres-Giner, S. Ductility and Toughness Improvement of Injection-Molded Compostable Pieces of Polylactide by Melt Blending with Poly(ε-Caprolactone) and Thermoplastic Starch. *Materials* **2018**, *11*, 2138.




https://doi.org/10.1021/acssuschemeng.0c09413
ACS Sustainable Chem. Eng. XXXX, XXX, XXX−XXX